A&A 425, 489–508 (2004)
DOI: 10.1051/0004-6361:20040312

Astronomy & Astrophysics

A search for late-type supergiants in the inner regions of the Milky Way⋆,⋆⋆

F. Comerón[1], J. Torra[2], C. Chiappini[3], F. Figueras[2], V. D. Ivanov[4], and S. J. Ribas[2]

[1] European Southern Observatory, Karl-Schwarzschild-Strasse 2, 85748 Garching, Germany
e-mail: fcomeron@eso.org
[2] Departament d'Astronomia i Meteorologia, Universitat de Barcelona, Av. Diagonal 647, 08028 Barcelona, Spain
e-mail: jordi@am.ub.es
[3] Osservatorio Astronomico di Trieste, Via G.B. Tiepolo 11, 34131 Trieste, Italy
e-mail: chiappin@ts.astro.it
[4] European Southern Observatory, Alonso de Cordova 3107, Santiago 19, Chile
e-mail: vivanov@eso.org

Received 21 February 2004 / Accepted 2 June 2004

Abstract. We present the results of a narrow-band infrared imaging survey of a narrow strip (12′ wide) around the Galactic equator between 6° and 21° of galactic longitude aimed at detecting field stars with strong CO absorption, mainly late-type giants and supergiants. Our observations include follow-up low resolution spectroscopy (R = 980) of 191 selected candidates in the H and K bands. Most of these objects have photometric and spectroscopic characteristics consistent with their being red giants, and some display broad, strong absorption wings due to water vapor absorption between the H and K bands. We also identify in our sample 18 good supergiant candidates characterized by their lack of noticeable water absorption, strong CO bands in the H and K windows, and HK_S photometry suggestive of high intrinsic luminosity and extinction reaching up to $A_V \simeq 40$ mag. Another 9 candidates share the same features except for weak H_2O absorption, which is also observed among some M supergiants in the solar neighbourhood. Interesting differences are noticed when comparing our stars with a local sample of late-type giants and supergiants, as well as with a sample of red giants in globular clusters of moderately subsolar metallicity and to a sample of bulge stars. A large fraction of the stars in our sample have CaI and NaI features markedly stronger than those typical in the local reference sample (both giants and supergiants), whereas the equivalent widths of the CO bands are similar or weaker. In this regard, our stars in the inner Milky Way disk display differences very similar to those identified by other authors between cool giants and supergiants near the galactic center and their counterparts in the solar neighbourhood. We propose that the systematic spectroscopic differences of our inner Galaxy stars are due to their higher metallicities that cause deeper mixing in their mantles, resulting in lower surface abundances of C and O and higher abundances of CN, which contribute to the strength of the CaI and NaI features at low resolution. Our results stress the limitations of using local stars as templates for the study of composite cool stellar populations such as central starbursts in galaxies.

Key words. stars: late-type – stars: supergiants – Galaxy: abundances – Galaxy: disk – Galaxy: stellar contents – Galaxy: structure

1. Introduction

Compared to the inner regions of nearby galaxies, for which a large amount of information available nowadays, the Population I component of the central kiloparsecs of the Milky Way is still relatively unknown. Visual extinction towards objects located in the galactic plane only a few kiloparsecs from the galactic center, typically reaching several tens of magnitudes, restricts the observations to the infrared and radio domains, or to X-rays or gamma rays for objects associated with high energy phenomena. Moreover, a variety of factors such as distance, extinction, field crowding, line-of-sight confusion, or absence of distinctive properties in the accessible wavelength range contribute to making difficult the identification or the detailed observation of individual objects. Observational programs such as large area surveys probing radio continuum and recombination line emission have supplied much of our present knowledge on the gas photoionized by massive stars (Lockman 1989; Helfand et al. 1992; Whiteoak 1992; Becker et al. 1989;

⋆ Based on observations collected at the Centro Astronómico Hispano-Alemán, Calar Alto, Spain; and at the European Southern Observatory, La Silla, Chile (programme 71.B-0274(A)).

⋆⋆ Full Table 1 and spectra in FITS format are only available in electronic form at the CDS via anonymous ftp to cdsarc.u-strasbg.fr (130.79.128.5) or via
http://cdsweb.u-strasbg.fr/cgi-bin/qcat?J/A+A/425/489

Kuchar & Bania 1992; McClure-Griffiths 2001; Kolpak et al. 2003), and on the nonthermal emission due to recent supernovae in the inner Galaxy (Leahy & Wu 1989; Green 1991, 2001). Molecular line emission surveys have provided an overall picture of the distribution and physical conditions of giant molecular clouds (Dame et al. 1987, 2001; Chiar et al. 1994; Bronfman et al. 1996, 2000; McQuinn et al. 2002), while mid-infrared surveys such as that carried out by IRAS have revealed a wealth of star forming sites (Wood & Churchwell 1989; Hughes & MacLeod 1989; Codella et al. 1995; Comerón & Torra 1996; Egan et al. 1998). Recent near-infrared surveys like DENIS (Ruphy et al. 1997; López-Corredoira et al. 2001; Van Loon et al. 2003), 2MASS (Alard 2001; Ojha 2001; López-Corredoira et al. 2002) or TMGS (López-Corredoira et al. 1999, 2001; Picaud et al. 2003) are yielding extensive lists of stellar objects suitable for studies of galactic structure. Valuable as all those observational approaches are, each one has its own limitations and needs to be complemented by the others to provide a global picture of the young component of the inner parts of our Galaxy. On the other hand, this young component is an excellent tracer of processes of primary importance concerning the structure and the composition of our Galaxy, such as the dynamical response of the disk to the central bar, the location of the spiral arms, the current star forming activity, or the radial dependency of the chemical composition, thus justifying the efforts leading to the characterization of its properties.

In this paper we present a study on a particularly promising, yet relatively unexploited, Population I tracer in the inner Galaxy. Late-type supergiant stars have interesting properties that make them particularly suitable for the study of aspects of the extreme Population I component that are either inaccessible or very elusive in other objects of similar age, such as the structure, kinematics, and chemistry of the young galactic disk, while their numerical abundance can provide a measurement of its present-day massive star formation rate. They have extremely bright magnitudes at infrared wavelengths, where the dust in the galactic disk is far less opaque than in the visible. As it turns out, a nearly *complete* census of late-type supergiants in our Galaxy is in principle a feasible task for a moderately large telescope equipped with a near-infrared camera, even if some of the targets may be as far away as 25 kpc and obscured by as much as 50 mag in V. While the bright magnitudes of supergiants facilitate detection, the infrared spectral properties of cool photospheres facilitate their identification in conveniently designed infrared surveys. The K-band spectra of objects with temperatures below ~3500 K are characterized by prominent CO bands appearing longwards of 2.29 μm, thus allowing the selection of candidate late-type stars (red giant branch (RGB) stars, long period variables in the asymptotic giant branch (AGB), and red supergiants) by comparing narrow band images centered respectively on and off the CO band region. In low- and medium- resolution spectroscopy, many narrow atomic features in the H and K bands allow further investigation of their intrinsic properties via their different sensitivities to temperature, surface gravity, metallicity, and surface abundances. Moreover, infrared observations of cool, luminous stars in the inner galactic disk provide actual, individual stellar templates suitable for the interpretation of the integrated spectrum of systems undergoing massive star formation, such as central starbursts and the environments of AGNs (e.g. Origlia et al. 1993; Kotilainen et al. 1996; Origlia & Oliva 2000; Förster-Schreiber et al. 2001; Alonso-Herrero et al. 2001), and are an important component in the modeling of the integrated light of entire systems (e.g. Fioc & Rocca-Volmerange 1997; Bruzual & Charlot 2003).

This paper describes a search for late-type luminous, obscured cool field stars in a 15°-long strip of the galactic plane of approximately 12′ width in galactic latitude, consisting of narrow-band imaging and low resolution follow-up spectroscopy of the best candidates identified. Although our focus is on the identification criteria of cool supergiants we have also obtained as a byproduct a large number of spectra of cool RGB and AGB stars in the same general direction, which can be a useful resource for studies of metallicity patterns across the inner galactic disk and for the construction of templates of spectra for integrated stellar populations.

The observations and data reduction process are described in Sect. 2. The results are presented in Sect. 3, where we discuss the properties of our sample and its comparison to those of reference samples containing objects in the solar neighbourhood, in the galactic bulge, and in relatively metal-rich globular clusters. We discuss criteria that allow the definition of a sample of red supergiant candidates and present a list of the best ones identified among our observed objects. Section 4 discusses one of the main results of our work, concerning systematic spectral differences that we find between our objects and those in the two reference samples. Section 5 summarizes our results.

2. Observations

2.1. Near-infrared imaging

2.1.1. Observing strategy and filter choice

The basis for our preliminary identification of possible cool supergiants consists of multiband images of narrow strips parallel to the galactic plane obtained with MAGIC, the near-infrared camera and spectrograph on the 1.23 m telescope at the German-Spanish Astronomical Center in Calar Alto. In imaging mode, MAGIC yields a scale of 1″15 per pixel resulting in a field of view of 4′9 × 4′9 over the 256 × 256 pixel^2 array. Our imaging observations were obtained on two separate observing runs, carried out respectively on 3−13 July 1998 and 19−21 June 2001.

The observations consisted of obtaining sequences of short exposures at positions separated by 1′ intervals along the galactic plane. Since the edges of the detector were aligned along the North-South and East-West directions and the series of images were obtained by moving the telescope along the galactic equator, stars lying at galactic latitudes near the edge of the coverage of the sequences were observed in fewer telescope pointings. At the beginning of each sequence the filter and the detector integration parameters were set, and then the sequence was started to obtain a total of 180 overlapping fields covering an arc of 3° in galactic longitude. The starting positions corresponded to galactic longitudes l = 6°, 9°, 12°, 15°, and 18°, and

galactic latitudes $b = 0'$, $+4'$, and $-4'$, thus allowing in principle overlap between contiguous sequences either in galactic longitude or latitude. Unfortunately, a major mechanical intervention on the mount of the 1.23 m telescope between our two runs produced a slight misalignment of its polar axis and an inaccurate pointing model in our run of 2001. As a result, the sequences starting at $b = -4'$ and the one at $l = 15°$, $b = +4'$ are not exactly parallel to the galactic equator and do not overlap over their entire lengths with contiguous sequences starting at the same galactic longitude.

Four filters were used: a CO filter centered at 2.295 μm with a relative width $\Delta\lambda/\lambda = 1\%$, a K-continuum narrow-band filter centered at 2.260 μm with $\Delta\lambda/\lambda = 2.6\%$, and the broad-band filters J (1.25 μm, $\Delta\lambda/\lambda = 24\%$) and H (1.65 μm, $\Delta\lambda/\lambda = 18\%$). The choice of narrow-band filters aims at allowing the detection of stars with large flux drops due to CO absorption, which is a characteristic feature of late-type photospheres, by comparing the images taken through the narrow-band CO and K-continuum filters (see below), while the broad-band filters were initially intended to locate objects in color−color and color−magnitude diagrams. Exposure times per telescope position were 9 s in the CO filter; 6 in the K-continuum filter; 4 in the H filter; and 8 in the J filter. These exposure times were obtained by stacking together as many individual exposures of 1 s each as needed. The exposure time per sky position is variable, as it depends on the number of telescope pointings containing that position as described above. It ranges from one to six times the exposure time per field, the latter value corresponding to stars lying close to the central galactic latitude of the sequence. Each frame was combined with the overlapping portion of the images taken before and after in the sequence to filter out remaining unmasked bad pixels or cosmic ray hits.

In general, preference was given to completing one sequence in all filters before proceeding to the next one, in order to have observations as closely spaced as possible. However this had to be often overridden because of visibility constraints as the regions imaged, lying at declinations between $-24°$ and $-10°$, are visible few hours per night from a Northern site (latitude 37°) like Calar Alto. As a consequence observations through the different filters are not consecutive, but separated by an interval of at most two days. Such time differences are nevertheless negligible by comparison to typical variability periods of evolved red stars, and we thus considered them entirely acceptable for the goals of our project.

2.1.2. Data reduction and calibration

The reduction of our imaging data, as well as of our spectra as described in Sect. 2.2, was carried out using IRAF[1] tasks and dedicated scripts. The images were reduced using dome flat fields in each filter; these were also used to construct bad pixel masks. Dark-subtracted, flat-fielded and masked images were sky-subtracted by constructing a sky frame made out of the 20 frames taken closest in time, conveniently median-averaged and with the stellar images removed by sigma clipping. Next, the images obtained within each of the $b = 0°$ sequences in the CO on-band filter, which we took as a reference, were mosaicked into a single large image. To this end, accurate offsets between consecutive pointings in a sequence were determined by automatically finding stars in the common area of overlapping images and using them as references. If a contiguous sequence (i.e., one starting at the same galactic longitude but a different latitude) was obtained during the same run, a similar procedure was used to align its component images with the reference $b = 0°$ sequence: the position of each individual image along the parallel sequence with respect to the reference one was determined by using stars in the overlapping areas. This was not possible when sequences starting at the same galactic longitude were obtained on different runs, due to the pointing model inaccuracy outlined above. In such cases the sequences obtained on the second run were combined separately. The combined image in the CO filter was used as the reference for the alignment of each frame in the other filters, thus avoiding large misalignments between images in different filters due to accumulated small errors in the registering of consecutive images in each of the filters.

Due to the crowdedness of the fields in the galactic plane and the undersampling of the point-spread function, digital photometry with an undersized aperture of 2 pixel (2″3) radius was found to provide the best results. To compensate for the variability of the sky transparency conditions and for the variable image quality during the execution of any given sequence, instrumental zeropoint variations along the sequence were determined by comparing the digital photometry of the brightest nonsaturated stars in the area common to each pair of overlapping frames. Zeropoints for each sequence in the J, H, and K-continuum bands were estimated by comparing our instrumental photometry of bright nonsaturated stars to the 2MASS catalog, assuming that the narrow-band K-continuum magnitude can be approximated by the broad-band 2MASS K_S magnitude.

The outlined procedure for photometric calibration is appropriate for yielding moderate accuracies in the J, H, and K-continuum bands that are sufficient for our purposes: a comparison of the instrumental and 2MASS magnitudes show a typical scatter of ∼0.1 mag around the average zeropoints, and a drift of the zeropoint of at most the same size at most along a given sequence. However, a scatter of that order is too large for the proper measurement of the flux drop due to CO absorption that we use as the primary criterion for selecting candidate cool stars. We thus used instead a self-calibrated method based on the fact that, in any random stellar field, most of the stars are expected to have a negligible drop in the flux at the position of the CO bands. We calculated local zeropoints of the photometric CO index (defined as $[CO]_{phot} = m(2.295) - m(2.26)$, where $m(2.295)$ and $m(2.26)$ are the magnitudes in the CO and K-continuum filters respectively) at each longitude by assuming that its value averaged over a large number of randomly selected stars must be very close to zero. This average was calculated considering the stars located within $|\Delta l| = 10'$ of each longitude point and on the same galactic longitude band, and

[1] IRAF is distributed by NOAO, which is operated by the Association of Universities for Research in Astronomy, Inc., under contract to the National Science Foundation.

with weights inversely proportional to the square of the probable error in magnitude of each contributing star. The calculation was done in two steps, the first including all the stars in the average and the second removing stars with a highly deviant $[CO]_{phot}$. In this way, cool stars that could skew the distribution of $[CO]_{phot}$ values could be selected, as they stood out because for them this index has as value above a given threshold, set above the average values of the surrounding stars.

A master list of detected stars was obtained by coadding the images taken in all the filters and running DAOFIND (Stetson 1987) on the combined image. With this master list of stellar positions, we performed digital photometry with DAOPHOT on the images in each filter to obtain the multiband photometry of each star detected in the combined image. Many stars were not detected in some bands, either because they fell just outside the edges of the image due to small differences between the starting position of the sequence in each filter, or because they were too faint in that filter to be detected, or because of confusion with a nearby source in the case of the images obtained under poorer seeing conditions. Finally, approximate stellar positions in J2000 coordinates were determined by using as a reference the positions of unobscured stars in our images that could be identified in the Digitized Sky Survey, and whose equatorial coordinates were available from the USNO astrometric catalog.

We must remark at this point that the conditions under which our observations were made resulted in an uneven depth of the catalog and other factors affecting its completeness. Seeing conditions during the execution of the observations ranged from $\sim 1''$ to over $3''$, thus resulting in a regional dependence of the source confusion limits. Likewise, part of our sequences was affected by the presence of high altitude dust combined with the need for observing often at high airmasses, producing regional dependencies of the depth of the frames. The net effects of all these circumstances are rather uncertain and difficult to quantify, a fundamental limitation of the present survey that must be kept in mind.

2.1.3. Properties of the photometrically selected sample

Our final catalog of detected sources contains 435 445 entries corresponding to stars with their magnitudes determined to an accuracy of better than 0.3 mag (excluding the contribution of the error in the zeropoint determination) in at least one of the J, H and K-continuum filters. This level is typically reached at $J = 15.5$, $H = 15.0$, $K = 13.0$. The shallower limit at K is due to the use of a narrow-band filter to estimate the K magnitude. On the other hand, deeper limits in J and H are needed to estimate the reddening towards the heavily obscured stars that are the object of our program. Figure 1 gives the histogram of source counts as a function of magnitude, excluding stars with $\sigma > 0.3$ mag in each band. The $[CO]_{phot}$ can usually be measured down to an accuracy of better than 0.1 mag for stars down to $K \simeq 10.0$, as estimated from the scatter of the measured $[CO]_{phot}$ values as a function of K. Although this is a rather modest limit in terms of depth, as we will see it is sufficient for our primary purpose of detecting late-type, distant supergiants. Our catalog contains 23 388 stars that have their $[CO]_{phot}$ indices determined to that level of accuracy. These stars are plotted in Fig. 2 to illustrate the changing behavior of $[CO]_{phot}$ with the $(H - K)$ color index. The top panel shows a sample with relatively blue $(H-K)$, which can be expected to be dominated by nearby stars with low reddening. The distribution of $[CO]_{phot}$ is approximately symmetric around a central value of 0 with a very minor fraction of the stars having an

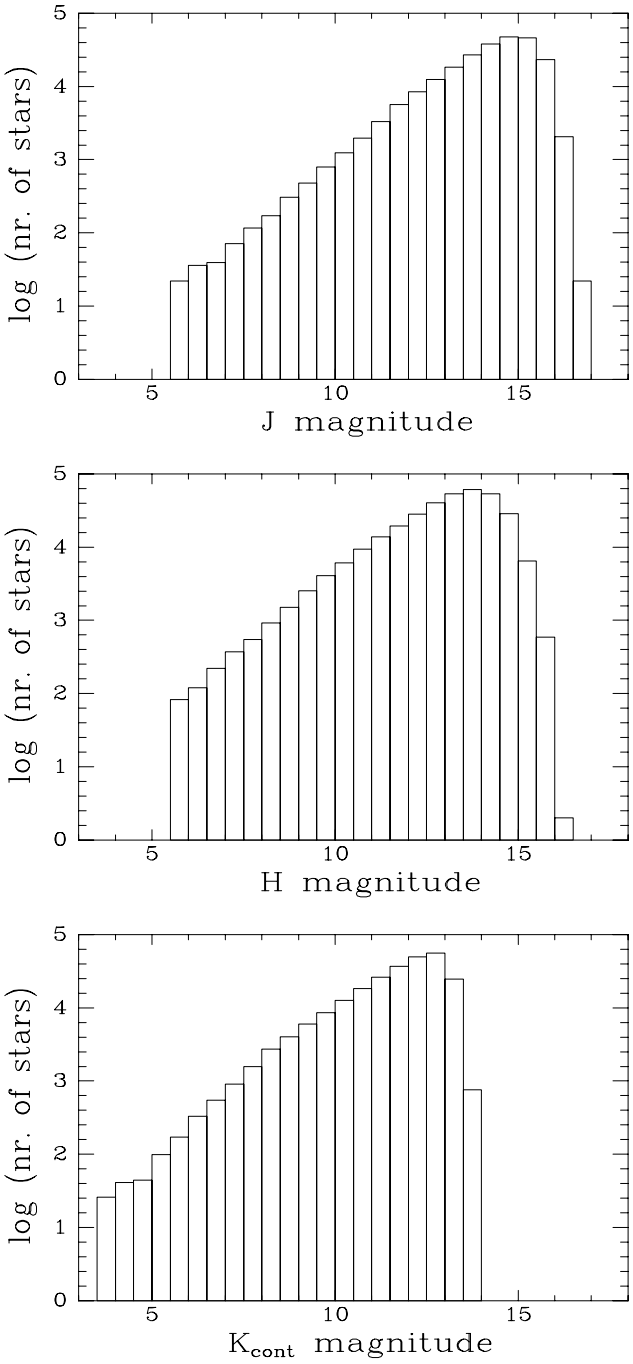

Fig. 1. Distribution of the magnitudes of the stars in our sample in the J, H, and K-continuum filters. Only stars with $\sigma < 0.3$ mag in the corresponding band are considered. The sharp cutoff at bright magnitudes indicates the saturation limit.

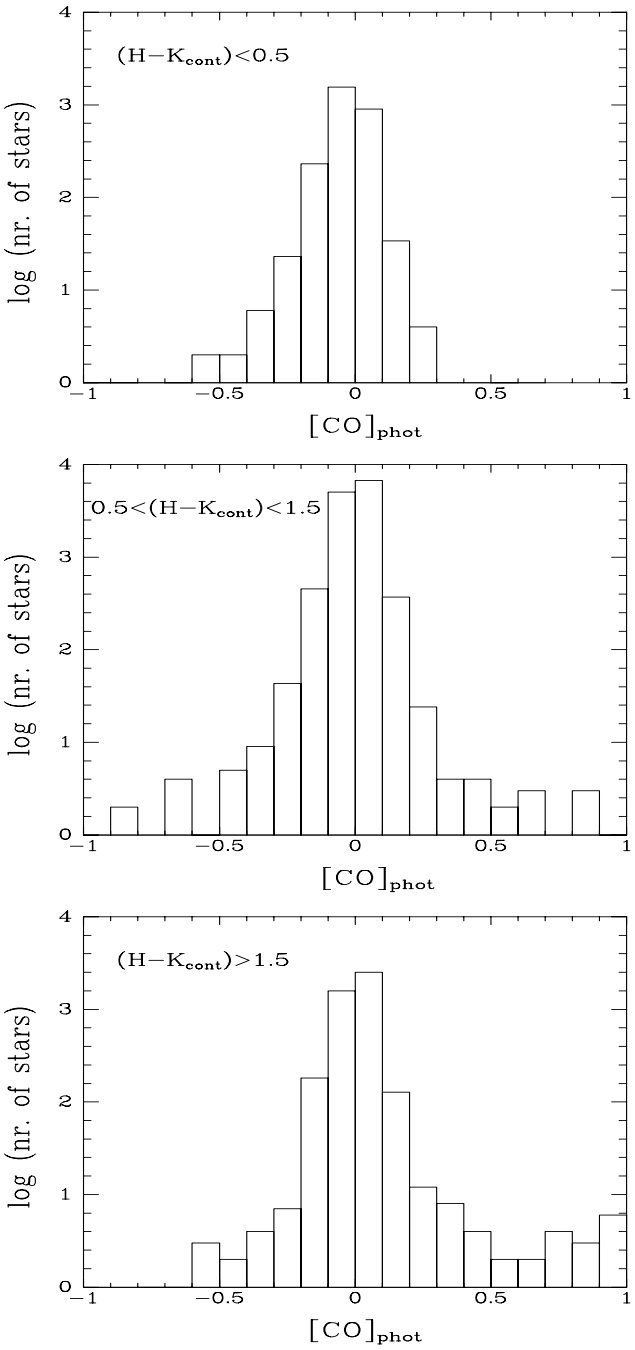

Fig. 2. The distribution of the $[CO]_{phot}$ index within three $(H-K)$ color bins, showing that cool stars are abundant among the most reddened ones. Only stars with $\sigma([CO]_{phot}) < 0.1$ have been plotted here. Note the use of a logarithmic scale on the vertical axis to enhance the wings of the distribution of indices, which is strongly peaked at $[CO]_{phot} = 0$.

index significantly different from that value, in most cases due to measurement errors caused by field crowding or the presence of nearby companions. Such measurement errors can be reasonably expected to affect stars regardless of their $(H - K)$. The second panel, with moderately reddened stars, has a very similar appearance but shows hints of skewness towards high values of $[CO]_{phot}$. The skewness is clearer when we consider the reddest stars in our sample, where we expect an increased contribution of luminous late-type stars that can be detected even at large distances and hence large amounts of foreground reddening.

2.1.4. Sample selection for spectroscopic follow-up

The imaging results described in the previous section were then used to select the best late-type cool star candidates to be observed spectroscopically. This sample was composed of stars having $[CO]_{phot} > 0.15$ and a K-continuum magnitude brighter than 10. Our selection was further refined by visually inspecting the images in which the stars selected according to these criteria appear, and discarding stars whose photometry was uncertain due to proximity to the edge of the image (where contamination by unfiltered bad pixels or cosmic rays was more frequent) or confused by the proximity to nearby bright sources. Such selection produced a list of 204 targets to be spectroscopically observed, out of which three were discarded because of the presence of a close companion that was not resolved in the images from Calar Alto. The star numbers given in Tables 1, 3, and 4 refer to the entry number in this list, which is sorted by increasing right ascension. The positions and broad-band photometry of the selected sources were obtained from the 2MASS Point Source Catalog, as its astrometric and photometric accuracy is better than that obtained for our sample with the procedures described above.

2.2. Near-infrared spectroscopy

The follow-up spectroscopy of the best candidate cool stars selected as described above was obtained using the SOFI near-infrared camera and spectrograph on the ESO New Technology Telescope on La Silla, Chile, on the nights of 11, 12, and 13 July 2003. The setup and exposure parameters used were identical for all the stars. We used the low-resolution red grism, which covers most of the H and K bands from 1.53 μm to 2.52 μm at a resolution $R = 980$ with the $0''6$-wide slit that we used. Four spectra were obtained for each star following an AB/BA pattern, with each spectrum being the on-detector stack of three exposures of 10 s each. The B5V star HD 169033, which lies near the arc of the galactic plane where our targets are located, was observed at periodic intervals of approximately one hour to sample the evolution of the telluric absorption in the proximity of our field. On the second night of our run we observed both HD 169033 and the solar analog HD 172411 (spectral type G3V) consecutively and near their culmination, in order to minimize effects in the telluric features affecting both.

For the reduction of the spectra, we started by canceling out the sky emission lines and the detector background by subtracting from each spectrum taken on the A position another taken on the B position, and vice versa. To correct for pixel-to-pixel variations we used a flat field obtained with the telescope enclosure closed, subtracting exposures taken with a continuum-emitting lamp respectively on and off.

The wavelength calibration was carried out in two steps. We first obtained an exposure of a xenon arc lamp, which produces a line spectrum conveniently sampling the wavelength interval

Table 1. Position, 2MASS photometry, and equivalent widths of selected features of all the observed stars.

						Equivalent widths				
Number	RA	Dec	K_S	$J-H$	$H-K_S$	CO(6, 3)	NaI	CaI	CO(2, 0)	$I(H_2O)$
	(2000)	(2000)		(2MASS)		(Å)	(Å)	(Å)	(Å)	(mag)
001	17:58:58.83	–23:43:03.7	10.36	2.11	0.87	5.65	4.34	3.71	15.64	–0.185
002	17:59:17.61	–23:48:02.3	9.93	2.09	0.92	8.34	4.04	3.25	21.00	–0.131
003	17:59:19.99	–23:49:34.8	9.86	1.23	0.53	2.34	2.31	2.70	11.33	–0.100
004	17:59:20.46	–23:51:11.7	9.53	2.47	1.14	9.45	5.11	3.42	21.99	–0.167
005	17:59:20.63	–23:34:01.1	9.64	2.21	0.95	7.84	4.32	3.59	20.44	–0.180

Note: the full version of this table is available from the CDS.

covered by our observations, immediately after observing one of our targets and keeping the instrument in the same position and setup, thus eliminating any possible flexure effects or inaccuracies in repositioning the slit. The arc lamp spectrum was wavelength-calibrated and the dispersion solution was applied to the sky spectrum of the object. In this way precise wavelenghts of the sky lines and line blends at the resolution of our observations were determined. The master calibrated sky spectrum was then used to wavelength-calibrate the rest of the observations. Each individual object spectrum was extracted, and the same aperture trace was used to extract the corresponding sky spectrum from an opposite frame in the AB/BA cycle. The lines identified in the master sky spectrum were then reidentified in the extracted sky spectrum at the position of the object and used to determine a new dispersion solution, which was then applied to the object spectrum. Finally, the four individual sky-subtracted, flat-fielded, wavelength-calibrated spectra of each object were combined into a single spectrum. An identical procedure was used for the telluric calibration star and the solar analog observations.

To remove telluric features, the spectrum of each program star was divided by the spectra of each of the telluric calibration stars observed on the same night. The residual left after dividing at the position of the strong CO_2 features in the 2.00−2.05 μm interval was used as a quality criterion to decide on the most suitable telluric calibration star to correct the telluric features in each program star. Since telluric features generally depend on both time and airmass the selected telluric calibration observation was often, but not always, the one obtained closest in time to the observation of the program star.

The last step was relative flux calibration and removal of photospheric features in the spectrum of the star used for telluric correction. This was carried out by dividing the consecutive observations of the telluric calibrator and the solar analog described earlier in this section, and multiplying this ratio by the flux-calibrated solar spectrum. The solar spectrum of Livingston & Wallace (1991) was used for this purpose, with its resolution degraded to match that of our observations, following the procedure described by Maiolino et al. (1996). The product of the telluric-over-solar analog ratio and the solar spectrum thus produced a multiplicative factor as a function of wavelength to be applied to our telluric-calibrated program objects in order to obtain their flux-calibrated spectrum in arbitrary units.

Of the 201 stars observed, 194 turned out to show obvious CO absorption bands characteristic of spectral types K or M. We discarded the 7 spectra of stars photometrically misclassified as cool stars, as well as 3 additional spectra of faint stars showing hints of CO absorption but having an insufficient signal-to-noise ratio, which either prevented the determination of the equivalent widths discussed in this paper or produced measurement errors not comparable to those of the other stars in the sample. Table 1 (available in full electronically only) contains the entire sample of 191 stars presented in this paper, listing their positions, 2MASS photometry, and measured equivalent widths of selected features (see Sect. 3.1). The numbering of the objects discussed in this paper refers to the entry number in that table. The complete collection of reduced spectra used in the following discussion is also available electronically.

As an additional step, we computed radial velocities for all our program stars by cross-correlating their K-band spectrum with a zero-velocity cool star template spectrum obtained by combining the spectra of M-type giant and supergiant stars in the atlas of Wallace & Hinkle (1997). Doppler-corrected spectra were produced in this way for all our program stars, as well as for the stars in the Lançon & Woods (2000) atlas that we use extensively as a reference in the present work (see Sect. 3.2). The Doppler-corrected spectra were the ones used for the derivation of the equivalent widths discussed in this paper. The accuracy of the radial velocities obtained is limited given the resolution of our spectra, and we estimate it to be approximately 30−40 km s^{-1} from the residuals of the dispersion solutions and the width of the cross-correlation peaks.

3. Results

3.1. Equivalent widths and spectrophotometric indices

At the relatively low resolution available, the main features that are visible in our K-band spectra are the CO bandheads redwards of 2.293 μm, as well as the NaI feature at 2.208 μm

and the CaI feature at 2.264 μm[2]. Other atomic lines such as those of FeI and MgI are also easily visible, as well as weaker features due to CN. More features appear in the *H* band. The reader is referred to Kleinmann & Hall (1986), Wallace & Hinkle (1997) and Hinkle et al. (1995) for detailed line identifications in these two bands. The overall shape of the continuum is strongly affected by the presence or absence of the broad wings of the water absorption band centered around 1.9 μm, where the separation between the *H* and *K* bands lies. Figure 3 shows some selected spectra representative of the variety found in our sample.

A considerable number of slightly different definitions of spectral passbands useful for the quantification of different features can be found in the literature (e.g. Lançon & Rocca-Volmerange 1992; Ramírez et al. 1997; Lançon & Wood 2000; Förster-Schreiber 2000; Frogel et al. 2001), which are normally defined in the most convenient way given the spectral resolution available. Our choice has been to adopt the *K*-band indices defined by Frogel et al. (2001) for the CaI, NaI, and CO(2, 0) features, which are also directly comparable to those used by Ramírez et al. (1997, 2000b). They thus allow a straightforward comparison between the spectral characteristics of our objects and those of the extensive samples of RGB stars observed by those authors in the solar neighbourhood (Ramírez et al. 1997), the galactic bulge (Ramírez et al. 2000b), and globular clusters (Frogel et al. 2001) (see Sect. 3.2). Moreover, we have defined additional passbands to measure SiI and CO(6, 3) features in the *H* band, and FeI, MgI in the *K* band. In all cases except for the *K*-band CO features the equivalent widths are measured with respect to the local continuum level interpolated between two featureless points on either side of the feature. The lack of a continuum longwards of 2.29 μm in our spectra forces us to use an extrapolation instead, using two continuum points at shorter wavelengths. The definition of the on- and off-feature bands used in this paper is given in Table 2. Note that the interpolation or extrapolation using two continuum bands makes the measured equivalent widths virtually insensitive to reddening, which is not the case for the $[CO]_{phot}$ defined earlier. Typical uncertainties in the equivalent widths that we measure in our spectra are ±0.5 Å, except for the CO(2, 0) band where we estimate ±1.0 Å due to the need to extrapolate from the bluer continuum.

The width of the wings of the H_2O feature separating the *H* and *K* bands requires a definition different from the equivalent widths discussed above to quantify their strength. We have thus defined a reddening-free water index, $I(H_2O)$, based on the comparison of the fluxes in two bands located in the blue and red wing of the feature and the approximate continuum level measured in unaffected parts of the *H* and *K* bands.

[2] These features receive their names from the atomic species that normally dominate the absorption at those wavelengths in spectra with resolutions $R \sim 1000$ or lower. However, higher resolution observations reveal contributions also by CN and atomic species that can become important below 4000 K (Ramírez et al. 1997), as discussed in Sect. 4. Although in this paper we refer to these features by their usual denomination in the literature (NaI, CaI), the reader should be aware that these species may not be the only ones contributing to their strength.

Table 2. Feature passbands and their reference continua.

Feature	Line/Band		Blue Cont.		Red Cont.	
	λ_0 (μm)	$\Delta\lambda$ (μm)	λ_0 (μm)	$\Delta\lambda$ (μm)	λ_0 (μm)	$\Delta\lambda$ (μm)
SiI	1.5898	0.0035	1.587	0.002	1.5953	0.0025
CO(6, 3)	1.620	0.0117	1.6140	0.006	1.6325	0.009
CN	2.1335	0.005	2.127	0.008	2.139	0.006
NaI	2.2075	0.007	2.194	0.006	2.215	0.004
FeI	2.2275	0.006	2.2145	0.006	2.2327	0.0045
CaI	2.2635	0.011	2.2505	0.011	2.271	0.002
MgI	2.2807	0.0035	2.277	0.004	2.2865	0.008
CO(2, 0)	2.2955	0.013	2.250	0.016	2.2875	0.007

Definition of passbands for measurement of H_2O band wings.

	λ_0 (μm)	$\Delta\lambda$ (μm)
f_H^C	1.675	0.05
f_H^L	1.755	0.05
f_K^L	2.075	0.05
f_K^C	2.255	0.05

Note: passbands for the measurement of the NaI, CaI, and CO(2, 0) features are defined as in Frogel et al. (2001) and Schultheis et al. (2003).

The locations and widths of these bands are also listed in Table 2, where f_H^L, f_K^L denote the fluxes in the *H*-band (blue) and *K*-band (red) wing of the feature, and f_H^C, f_K^C are the respective continuum fluxes. Figure 4 shows the position of the bands used to measure $I(H_2O)$. Assuming that the extinction has a wavelength dependence of the form $A_\lambda \propto \lambda^{-1.7}$ (Mathis 1990), the quantity

$$I(H_2O) = -2.5 \log \frac{f_H^L}{f_H^C} - 2.081 \log \frac{f_K^L}{f_K^C} \quad (1)$$

is thus a reddening-free measurement of the depression in flux due to water vapour absorption on both sides of the gap separating the *H* and *K* bands, which we express in magnitudes for convenience.

3.2. The reference samples

Low- and medium-resolution atlases of cool stars in the infrared have been presented in a number of studies (e.g. Kleinmann & Hall 1986; Lançon & Rocca-Volmerange 1992; Dallier et al. 1996; Wallace & Hinkle 1996, 1997; Meyer et al. 1998; Förster-Schreiber 2000; Ivanov et al. 2004; see this latter reference for a more exhaustive list of relevant work), with the twofold purpose of providing a tool both for the classification of individual objects and for the construction of templates of integrated spectral energy distributions for population synthesis analyses. Among these atlases, a particularly suitable one for the investigation of the properties of our sample is provided by the extensive collection of cool stellar spectra in the visible and the near infrared published by Lancon & Wood (2000, hereafter

Table 3. Candidate supergiants with no H_2O absorption wings.

						Equivalent widths				
Number	RA	Dec	K_S	$J-H$	$H-K_S$	CO(6, 3)	NaI	CaI	CO(2, 0)	$I(H_2O)$
	(2000)	(2000)		(2MASS)		(Å)	(Å)	(Å)	(Å)	(mag)
011	17:59:36.64	–23:41:16.3	7.33	2.95	1.47	11.36	4.38	4.41	28.87	–0.197
026	18:02:45.68	–22:24:40.2	8.90	3.25	1.60	9.67	4.60	3.63	22.17	–0.179
059	18:07:15.19	–20:19:11.6	7.76	2.67	1.43	8.92	4.37	3.61	19.57	–0.187
063	18:07:50.04	–20:09:12.5	7.41	1.79	0.87	7.34	4.48	4.07	20.38	–0.190
072	18:08:54.05	–19:46:14.1	10.03	3.18	2.58	9.91	4.59	3.87	25.91	–0.215
091	18:13:16.80	–18:00:49.2	9.25	3.76	2.49	9.39	5.42	5.95	25.31	–0.218
094	18:14:21.54	–17:28:59.4	9.99	4.04	2.42	9.83	5.07	5.51	23.95	–0.167
114	18:16:30.34	–16:26:56.5	8.20	2.72	1.30	10.68	5.27	4.45	24.30	–0.117
123	18:16:41.18	–16:22:49.5	7.12	1.88	0.84	9.48	4.15	5.03	23.01	–0.108
128	18:17:14.03	–16:07:58.6	8.12	2.61	1.23	9.97	4.84	4.48	22.36	–0.132
130	18:17:18.60	–16:04:53.0	9.53	3.77	1.74	8.75	4.22	3.57	24.06	–0.246
131	18:17:22.53	–16:06:31.0	8.43	2.66	1.22	9.50	5.38	5.21	22.48	–0.160
136	18:17:27.66	–16:04:14.9	8.62	3.36	1.58	10.69	5.46	4.76	24.01	–0.196
143	18:17:36.86	–16:06:59.8	9.83	4.43	2.23	10.55	5.31	5.23	23.54	–0.232
145	18:17:41.07	–15:55:26.4	9.89	1.86	2.26	8.27	5.85	5.20	24.89	–0.230
161	18:20:57.79	–14:43:28.4	10.12	3.89	2.36	11.81	4.32	2.79	21.85	–0.239
167	18:23:17.55	–13:47:16.0	6.96	2.17	1.03	9.78	5.37	5.87	26.34	–0.135
178	18:24:37.26	–12:54:04.0	9.55	4.54	2.45	9.25	5.23	4.37	25.15	–0.108

Table 4. Candidate supergiants with weak H_2O absorption wings.

						Equivalent widths				
Number	RA	Dec	K_S	$J-H$	$H-K_S$	CO(6, 3)	NaI	CaI	CO(2, 0)	$I(H_2O)$
	(2000)	(2000)		(2MASS)		(Å)	(Å)	(Å)	(Å)	(mag)
064	18:07:50.72	–20:04:09.2	7.77	2.91	1.58	9.13	4.21	3.34	19.58	–0.063
070	18:08:37.35	–19:50:05.3	8.40	3.24	1.57	9.05	4.50	3.68	25.41	–0.059
074	18:09:37.50	–19:28:27.1	10.07	4.11	2.03	7.87	5.16	5.06	26.27	–0.098
097	18:14:53.10	–17:00:51.3	8.28	2.75	1.41	11.40	5.12	3.90	24.57	–0.050
121	18:16:38.18	–16:23:34.0	9.09	3.12	1.62	10.43	5.76	4.23	25.73	–0.024
125	18:16:55.97	–16:09:54.3	5.15	1.91	0.91	9.46	5.09	4.59	21.99	–0.031
152	18:18:05.31	–15:57:19.4	6.48	2.76	1.44	9.66	5.59	4.60	24.29	–0.035
184	18:25:11.20	–12:28:40.2	8.33	3.02	1.43	10.04	5.12	4.40	22.48	–0.049
194	18:27:39.07	–11:39:23.0	7.09	2.11	1.03	7.74	4.59	4.10	23.88	–0.045

LW2000). Their sample provides a wide variety of spectra corresponding to different classes of luminous cool stars in different environments such as the solar neighbourhood, the galactic bulge, and the Magellanic Clouds, and includes multiepoch observations for a large number of variable stars. Its resolution, $R = 1100$, closely matches that of the spectra presented in this paper, thus facilitating a direct comparison (see Fig. 5). Classes represented in LW2000 include supergiants, thermally pulsating AGB stars of high and low amplitudes, non-pulsating RGB stars, and carbon stars.

We have used the spectra from LW2000 for which those authors present observations in the H and K-band that belong to the samples of supergiants, oxygen-rich variables, bulge giants, and non-pulsating RGB stars. Unfortunately, few spectra in the H and K bands are available for the latter class of objects in the LW2000 sample. This shortcoming can be largely circumvented by adding the collection of equivalent widths of the NaI, CaI, and CO(2, 0) features in the K-band spectrum of bright giants measured by Ramírez et al. (1997) in spectra having a resolution similar to ours. We have also used the lists of equivalent widths of the same features in Ramírez et al. (2000b) for a sample of over 100 bulge RGB stars, and of RGB stars in the most metal-rich globular clusters observed by Frogel et al. (2001), namely NGC 5927 ([Fe/H] = −0.37), NGC 6440 ([Fe/H] = −0.34), NGC 6528 ([Fe/H] = −0.17), and NGC 6553 ([Fe/H] = −0.25). Low-metallicity objects such as those in the Magellanic Clouds sample of LW2000 are not expected to be significantly represented among our

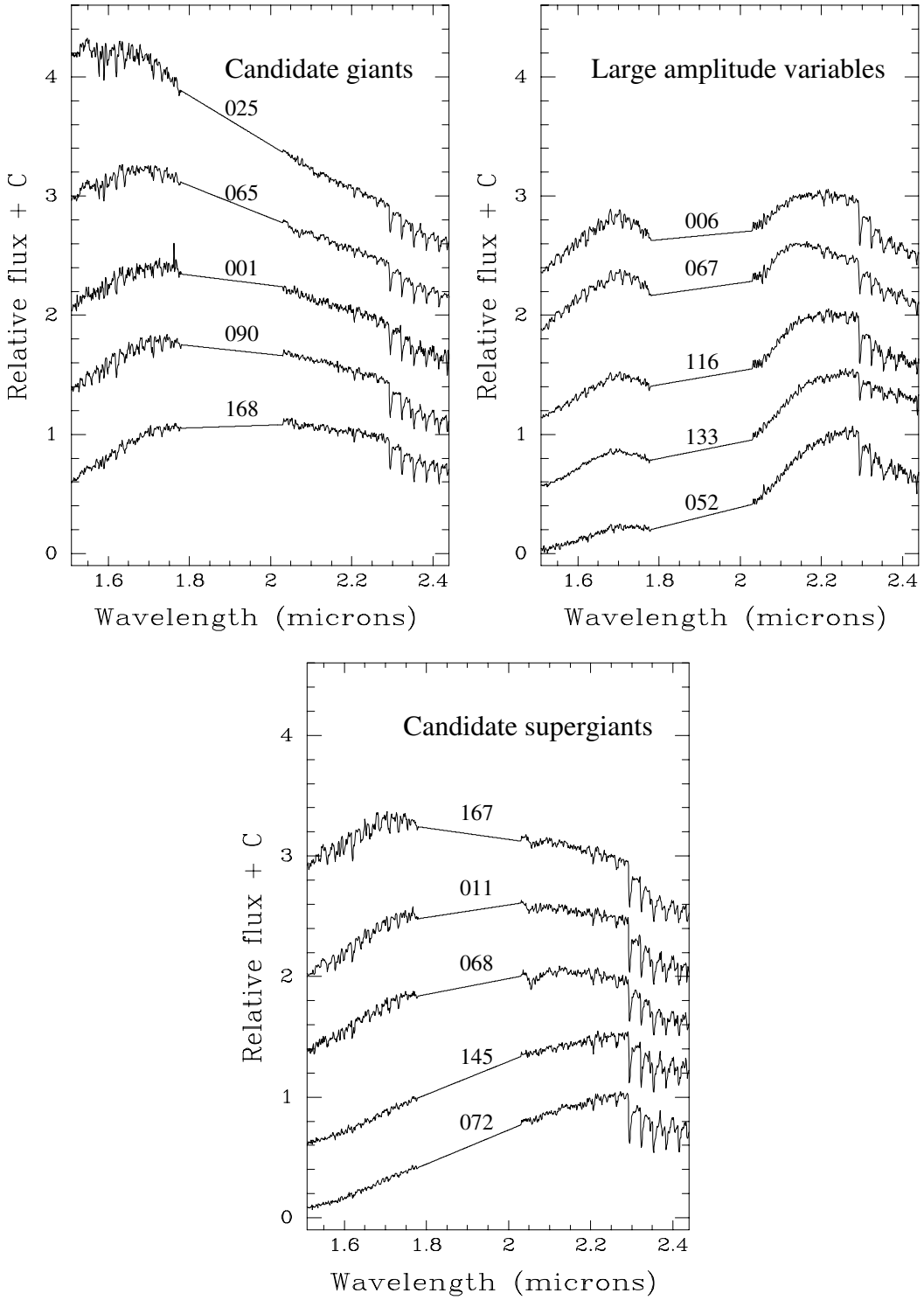

Fig. 3. Representative examples of cool stellar spectra found in our sample. The interval between 1.80 μm and 2.05 μm is contaminated by strong telluric absorption bands and has been cut off. The spectra in the top left panel show relatively strong CO absorption bands, but no signs of depression due to the wings of the broad water feature centered near 1.9 μm. The top right panel shows a sample of stars with similarly strong CO, but now also with a conspicuous H_2O feature, that we classify as large amplitude variables following LW2000. The stars in the bottom set of spectra are drawn from the sample of candidate supergiant stars (see Sect. 3.7). The spectra are normalized to the flux between 2.20 and 2.25 μm, and the offsets between consecutive spectra are 0.5 in these normalized flux units.The number accompanying each spectrum refers to the entry number in Table 1.

inner galactic disk objects, and have not been considered here. Likewise, there are clearly no carbon-rich stars in our sample (they would be easily distinguishable thanks to the strong C_2 feature at 1.77 μm) and we have thus excluded the objects of that class in the LW2000 atlas from comparison with our results.

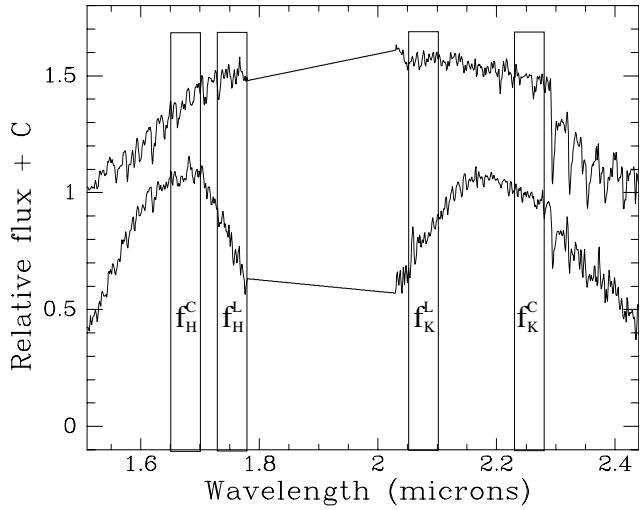

Fig. 4. The positions of the spectrophotometric bands defined in Sect. 3.1, plotted on representative spectra from our sample to show their usefulness in measuring the flux depression caused by strong water band wings.

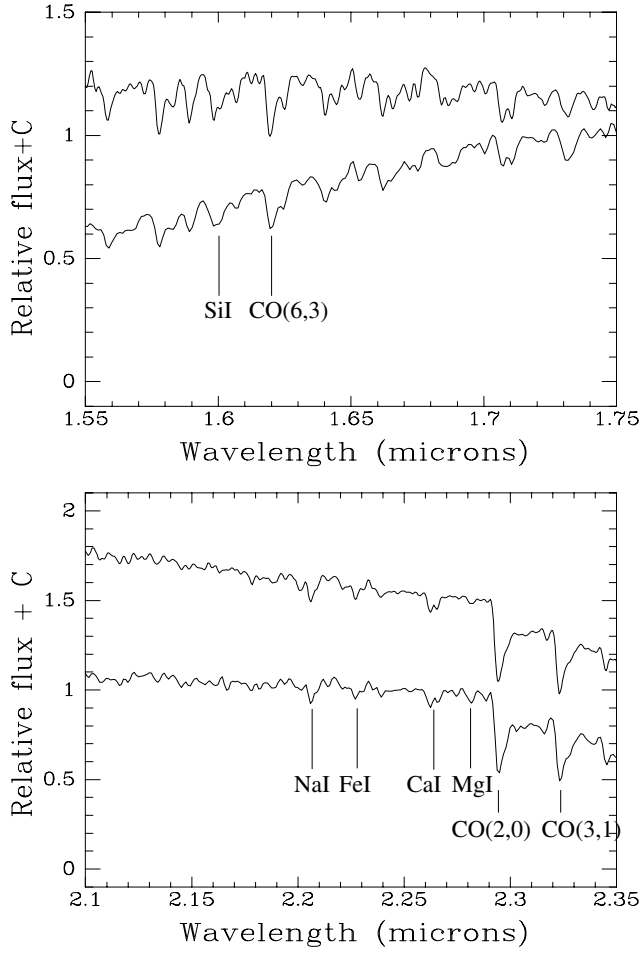

Fig. 5. A comparison between the *H* and *K* spectra of one supergiant from the LW2000 library of spectra (above) and one supergiant candidate from our sample (below), showing their similar resolution and quality. The comparison also shows the reality of most of the features that can be seen in our spectra. The difference in continuum slopes, especially in the *H* band, is due to the higher extinction towards the star of our sample. The features listed in Table 2 are noted.

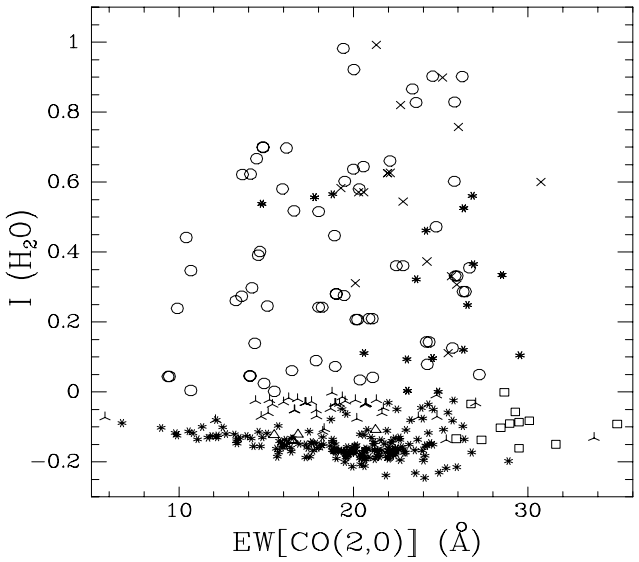

Fig. 6. *EW*[CO(2, 0)] vs. $I(H_2O)$ diagram for all the stars in our sample (eight-pointed asterisks), compared to the different classes of cool stars of LW2000: non-pulsating red giants (triangles), supergiants (squares), bulge giants (crosses), and oxygen-rich variables, separated between those having strong (circles) and weak (three-pointed asterisks) water absorption.

3.3. The H_2O vs. CO diagrams

A first classification of a sample of cool luminous star can be established on the basis of the relative importance of the most prominent molecular features in the *H* and *K* bands due to water and carbon monoxide. CO is to a first approximation a temperature indicator with the depth of the bands increasing as the temperature decreases. However, the depth of the CO bandhead at 2.293 μm is also sensitive to the surface gravity and is often used as a discriminator between giants and supergiants at a given temperature (e.g. Kleinmann & Hall 1986; Förster-Schreiber 2000; Ivanov et al. 2004). The CO band intensity is also sensitive to the carbon abundance in the atmospheres of oxygen-rich stars and is thus an indicator of the importance of the dredge-up processes in the post-main sequence evolution of the star (Carr et al. 2000). On the other hand, strong H_2O absorption is formed in the cool, dense outer layers of large amplitude Mira-type and semiregular variables possessing very extended atmospheres with a complicated structure determined by shocks propagating through them (Bessell et al. 1989, and references therein), and can be used as a discriminator between pulsating AGB stars and supergiants (Lançon & Rocca-Volmerange 1992), which have overlapping luminosity ranges.

Figure 6 shows the distributions of our sample and the LW2000 one in the CO(2, 0)-H_2O diagram. The apparent overabundance of objects with strong water absorption in LW2000 is largely due to the fact that we have plotted in the diagram every single observation of each object in LW2000 as a separate point; therefore, for any given star observed at different phases by LW2000 there are multiple entries in the diagram. Figure 6 shows that our sample is strongly dominated by objects with the spectral characteristics of non-pulsating

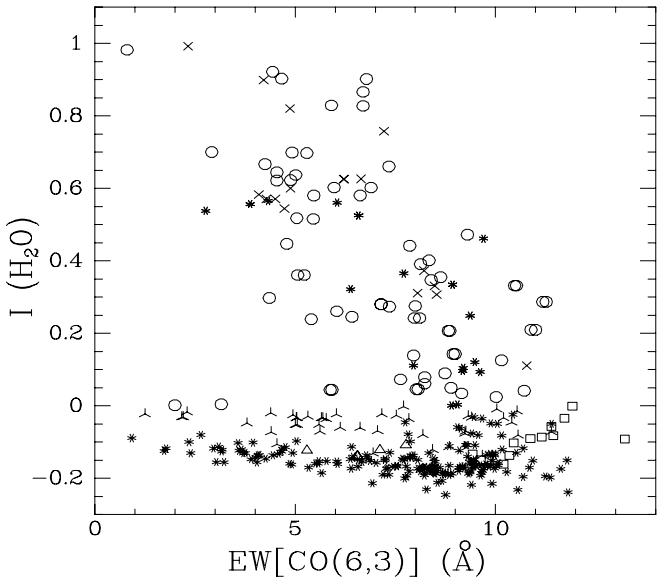

Fig. 7. *EW*[CO(6, 3)] vs. $I(H_2O)$ diagram comparing the stars in our sample with those of LW2000. Symbols are as in Fig. 6.

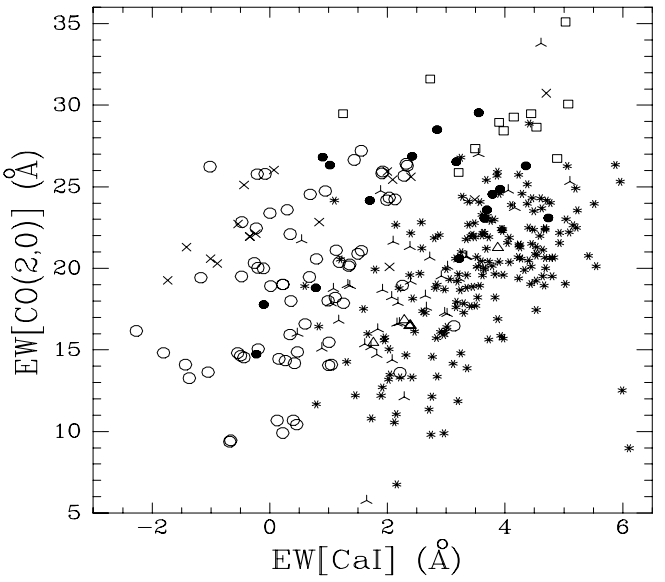

Fig. 8. *EW*[CaI] vs. *EW*[CO(2, 0)] diagram comparing the stars in our sample with those of LW2000. Symbols are in general as in Fig. 6, but now the stars of our sample with $I(H_2O) > 0$ are marked as filled circles. Note the offset between the mean distribution of stars of our sample and other reference samples.

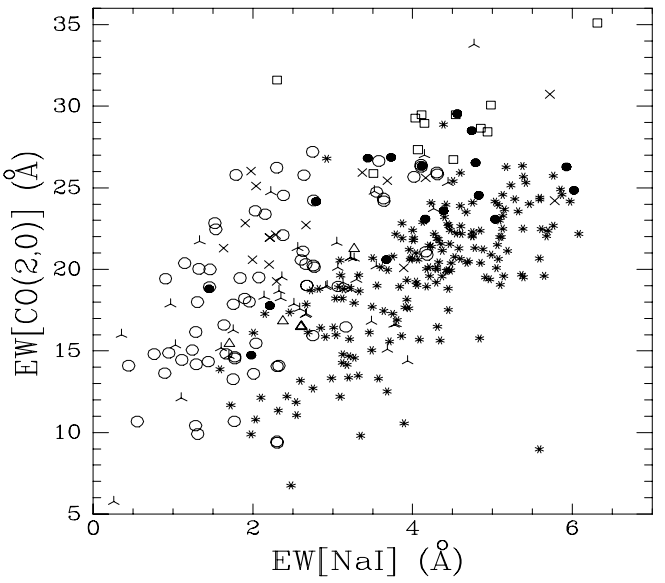

Fig. 9. *EW*[NaI] vs. *EW*[CO(2, 0)] diagram comparing the stars in our sample with those of LW2000. Symbols are as in Fig. 8. Like in Fig. 8, there is a clear offset between the mean distribution of stars of our sample and that of other reference samples. Note that a large fraction of our stars reach *EW*[NaI] values higher than those of most local supergiants.

stars that occupy the *locus* of red giants and supergiants. The small scatter of $I(H_2O)$ for objects spanning a wide range of extinction confirms that the extinction law chosen to derive Eq. (1) yields a reddening-free index, whereas its steady decline between *EW*[CO(2, 0)] = 10 Å and 20 Å is due to the progressive departure of the *H* and *K* band spectrum from a Rayleigh-Jeans shape as the temperature decreases and the depth of the CO bands increases. Most of our objects have moderate values of *EW*[CO(2, 0)] that are generally well below those of the sample of LW2000 supergiants, a feature that we will consider in the coming sections. Finally, the objects with strong water absorption have a preference towards high *EW*[CO(2, 0)], unlike in the LW2000 sample where large positive $I(H_2O)$ indices are present over the whole range of *EW*[CO(2, 0)] considered. The trend in our sample is qualitatively similar to that observed in Fig. 13 of Lançon & Rocca-Volmerange (1992) where their objects split along two branches (corresponding to RGB stars and supergiants) at the highest *EW*[CO(2, 0)], although we do not find the gap between the two branches suggested by the results of those authors. Unfortunately, no information on the H_2O depression is available in the data published by Ramírez et al. (1997) given their wavelength coverage, which is restricted to the red part of the *K* band.

Figure 7 is analogous to Fig. 6, but for the CO(6, 3) band at 1.62 μm instead of the CO(2, 0) band. Again cool supergiants of the LW2000 sample occupy the region of highest CO absorption, now with a larger overlap with our sample. A difference with Fig. 6 is that objects with $I(H_2O) > 0$ now populate a broad but clearly defined band so that the objects with the strongest water absorption tend to have the lowest *EW*[CO(6, 3)]. The same behaviour in this respect can be seen in the LW2000 sample and in ours. A closer examination shows that not only the CO(6, 3) band, but all the features in the *H* band are weaker among the stars with strong water band wings, indicating the existence of significant veiling correlated with the strength of the water feature. Some degree of veiling in the *K* band as well may be responsible for the relatively weak CaI and NaI features of stars with $I(H_2O) > 0$ in Figs. 8 and 9.

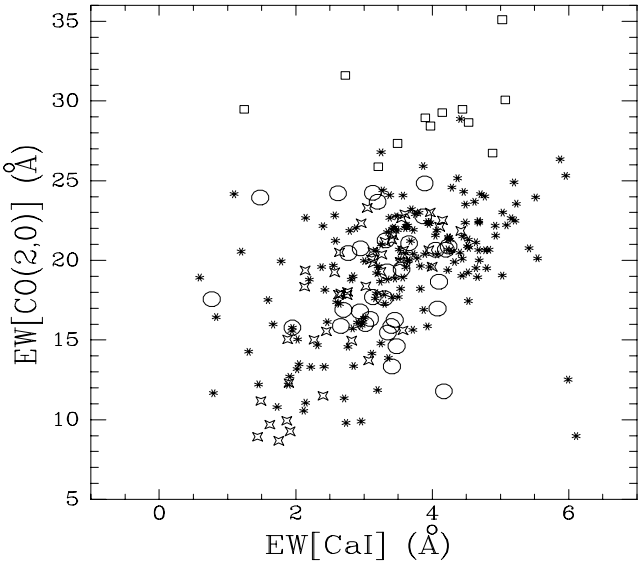

Fig. 10. Same as Fig. 8, but now comparing our sample to that of RGB stars in the solar neighbourhood from Ramírez et al. (1997; four-pointed stars) and in relatively metal-rich globular clusters from Frogel et al. (2001) (open circles). The LW2000 sample of supergiants (open squares as in previous figures) is also included.

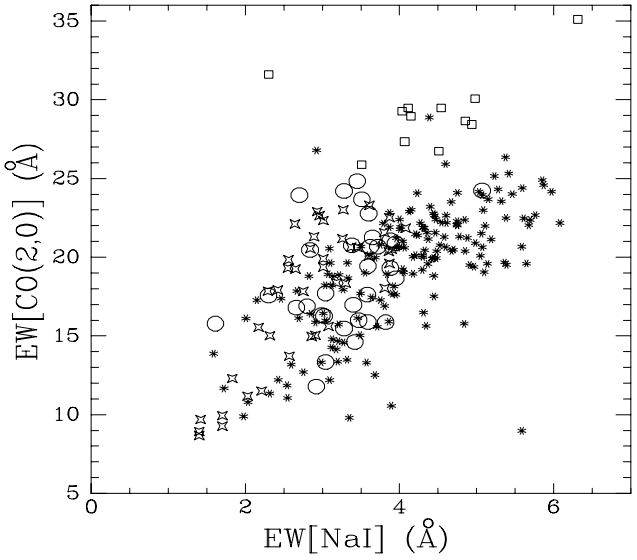

Fig. 11. Same as Fig. 9, but now comparing our sample to that of RGB stars in the solar neighbourhood from Ramírez et al. (1997; four-pointed stars) and in relatively metal-rich globular clusters from Frogel et al. (2001) (open circles). The LW2000 sample of supergiants (open squares as in previous figures) is also included. Note that most of our stars have *EW*[NaI] greater than those of the coolest RGB globular cluster stars.

3.4. The NaI and CaI features

Diagrams combining absorption in atomic lines and molecular bands having different dependencies on temperature, surface gravity, and metallicity offer in principle important diagnostics on the intrinsic properties of samples of individual cool stars and of composite populations, and have been discussed in a number of studies (see Ivanov et al. 2004 for a recent, comprehensive review). A comparison between our sample in the inner Galaxy, the sample of LW2000, and the samples of RGB stars in the solar neighbourhood, the bulge, and globular clusters described in Sect. 3.2 can provide insight in possible intrinsic differences of both populations and the way they are reflected in measurable spectral features.

We have plotted in Figs. 8 and 9 the relationship between the NaI and CaI features and the CO(2, 0) bandhead. In particular, the combination of the strength of a feature essentially dependent on the temperature such as CaI and one that combines dependence on temperature and surface gravity such as CO(2, 0) has been proposed as a luminosity class discriminator (Förster-Schreiber 2000; Ivanov et al. 2004).

Figures 8 and 9 do not show tight overall correlations for the LW2000 sample, mainly due to its high percentage of AGB stars whose complex, time-dependent atmospheric structure is expected to blur the correlations. However, local supergiants dominate in a well defined region of the diagram characterized by the strongest absorptions in both the CaI and NaI features and CO(2, 0).

The loose correlation between the CaI or NaI features and CO(2, 0) is much more apparent when only RGB stars and supergiants are considered, as shown in Figs. 10 to 13, where our sample is compared to the local supergiants of LW2000 and the RGB stars in the solar neighbourhood (Ramírez et al. 1997), the galactic bulge (Ramírez et al. 2000b), and the

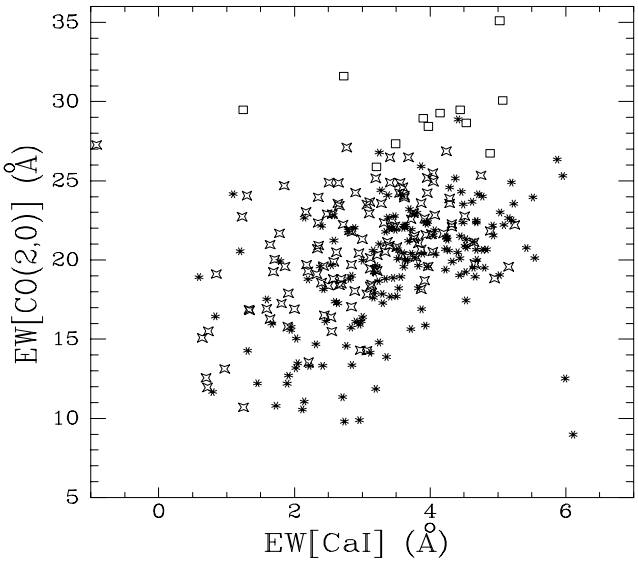

Fig. 12. Same as Fig. 8, but now comparing our sample to that of RGB stars in the galactic bulge from Ramírez et al. (2000b; four-pointed stars). The LW2000 sample of supergiants (open squares as in previous figures) is also included.

relatively metal-rich globular clusters of Frogel et al. (2001). Clear systematic differences are noted between the stars in our sample on one side, and the local RGB sample of Ramírez et al. (1997) and the sample of RGB stars in globular clusters of Frogel et al. (2001) on the other, in the sense that the equivalent widths of the atomic features in our sample extend to higher values. Local RGB stars occupy essentially the same region of the diagrams presented in Figs. 10 and 11 as RGB stars in globular clusters, which are also plotted in those

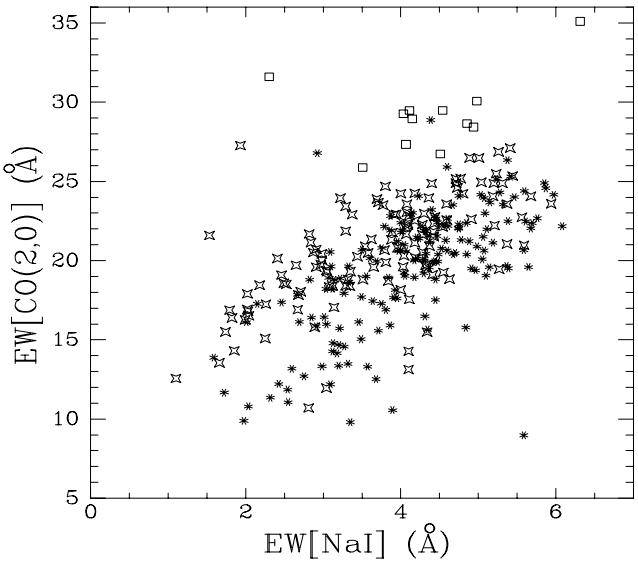

Fig. 13. Same as Fig. 9, but now comparing our sample to that of RGB stars in the galactic bulge from Ramírez et al. (2000b; four-pointed stars). The LW2000 sample of supergiants (open squares as in previous figures) is also included. Note that most of our stars have EW[NaI] greater than those of the coolest RGB globular cluster stars.

figures. This is especially clear in the NaI vs. CO(2, 0) diagram, where the overlap in EW[NaI] of the giants and supergiants of the reference samples is minor, and where only one RGB star belonging to NGC 6528 (the highest metallicity cluster in the Frogel et al. (2001) sample) appears with EW[NaI] > 4.0 Å. The strengths of the CO(2, 0) bandhead in our stars are otherwise similar to, or only slightly exceeding, the ones of the coolest RGB stars in the local and globular cluster samples. On the other hand, the galactic bulge sample has overall characteristics much closer to those of our objects, as shown in Figs. 12 and 13. The largest measured equivalent widths of the CO(2, 0) feature are similar to those of the local RGB star sample, which may be explained by their proximity to saturation and subsequent insensitivity to metallicity differences. However, RGB stars in the bulge do reach the high CaI and NaI equivalent widths that we measure in our sample and their *loci* in those diagrams has a much broader, although not complete, overlap with the one of our sample. The overlap with this sample is nevertheless poorer at low equivalent widths, where the local RGB stars from Ramírez et al. (1997) rather than bulge RGB stars tend to populate the region occupied by the stars of our sample. This is to be expected since stars with lower equivalent widths are hotter, and therefore intrinsically fainter and more nearby on average as indicated by the lower reddening of their colors, and can thus be considered as an extension of the local sample.

Metallicity differences between RGB stars in the solar neighbourhood and in the bulge are the most obvious candidate to produce the systematic shifts between samples in the equivalent width diagrams. The quantification of these differences from low resolution spectra is however difficult, as the use of relationships calibrated for globular clusters implies their extrapolation outside their strict range of applicability (temperatures, luminosities, metallicities, feature strengths, star formation and chemical pollution environments...) and even become dependent on the functional form adopted for the relationships, as illustrated in Fig. 6 of Ramírez et al. (2000b). Moreover, the low resolution spectrum may also be determined by other effects that mimic metallicity effects, as discussed in Sect. 4.1.

3.5. Color–magnitude diagram and luminosities

The obvious differences in the intrinsic properties of the local giants and the ones in the inner galactic disk, represented by our objects and the bulge sample of Ramírez et al. (2000b), respectively, leads us to be cautious about possible differences also existing between local supergiants and those in the inner Galaxy that may render inapplicable the spectroscopic criteria allowing a separation between giants and supergiants in the solar neighbourhood. Indeed, such criteria do not seem to apply at least to giants and supergiants at the galactic center, as concluded by Schultheis et al. (2003) from their near-infrared study of a sample of cool, luminous stars detected in the ISOGAL survey (Omont 1996) with spectra obtained with the same instrumentation as ours. Schultheis et al.'s identification of four very likely cool supergiants rests on their derived luminosities, which they estimate based on the assumption that all the sources in their sample lie at the distance of the galactic center. This is a reasonable working hypothesis in their case, given the high density of sources detected within a radius of less than 1°5 from the galactic center in which foreground contamination is expected to be negligible. Unfortunately we cannot make a similar assumption on the distance, and are thus forced to examine more indirect means of estimating the luminosity of our stars in order to assess the possible presence of supergiants among them, without relying on spectroscopic criteria derived from the solar neighbourhood.

Figure 14 suggests that it is possible to make a rough luminosity estimate based on the 2MASS photometry alone. The figure plots the position of all objects in our sample in a $(H - K_S, K_S)$ color−magnitude diagram, including AGB stars characterized by their prominent vapour bands (see Sect. 3.3), which are marked as full circles. These stars are expected to be long-period variables roughly following the period-luminosity relationship for Miras and semiregular variables, which has recently been reexamined by Knapp et al. (2003) using Hipparcos parallaxes. Their absolute magnitudes range from $M_K \simeq -6.4$ for the shortest periods to $M_K \simeq -8.2$ at the tip of the AGB, and thus overlap with the absolute magnitude range of cool supergiants, from which they can otherwise be easily separated spectroscopically. Concerning the brightest AGB stars, their absolute M_K magnitudes are expected to depend on the metallicity, primarily due to the cooler temperatures reached at the tip of the RGB by the most metal-rich populations as compared to others of lower metallicity, which result in a greater K-band bolometric correction (Houdashelt et al. 2000) combined with an essentially metallicity-independent bolometric luminosity (Sweigart et al. 1990). A moderate extrapolation of the metallicity-M_K relationship established by Ferraro et al. (2000) from a sample of globular clusters to the solar metallicities indicates an expected $M_K = -7$ for the brightest RGB stars,

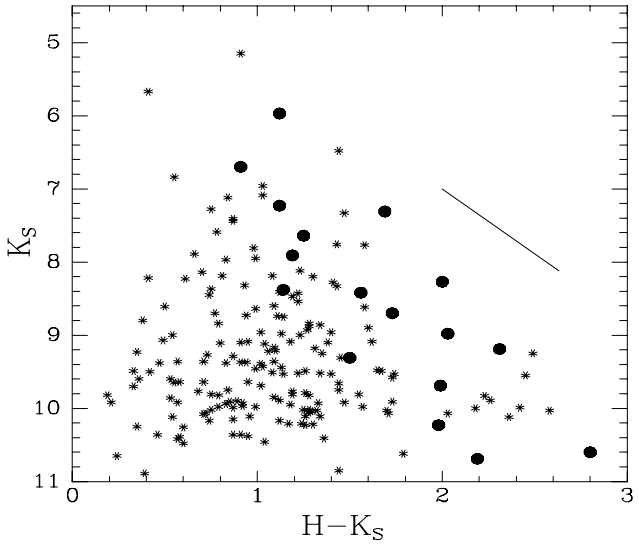

Fig. 14. Color−magnitude diagram for the stars in our sample. Filled circles represent stars with $I(H_2O) > 0$ (large-amplitude variables), expected to be intrinsically very luminous. Magnitudes are from 2MASS. The straight line represents the displacement due to an extinction of $A_V = 10$, using the Rieke & Lebofsky (1985) extinction law.

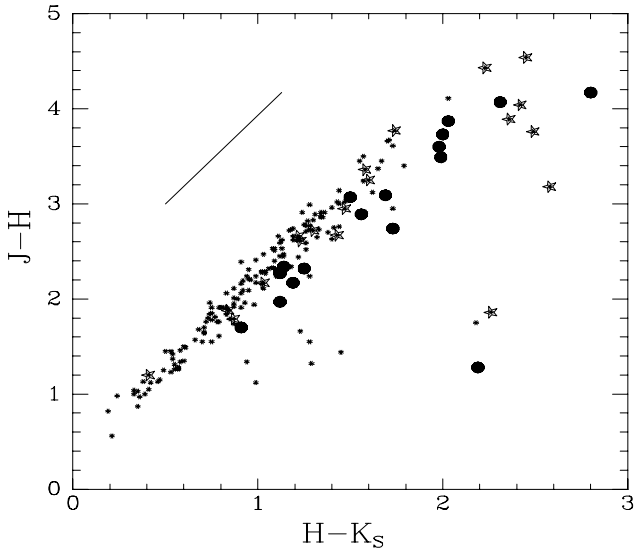

Fig. 15. Color−color diagram for the stars in our sample, based on 2MASS magnitudes. Filled circles represent stars with $I(H_2O) > 0$ (large-amplitude variables). Five-pointed stars represent our best supergiant candidates (see Sect. 3.7). Note that the J magnitudes of stars with very red ($H-K_S$) colors are often unreliable due to the likelihood of contamination by nearby stars that are brighter in J. The straight line represents the displacement due to an extinction of $A_V = 10$, using the Rieke & Lebofsky (1985) extinction law.

thus overlapping with the absolute magnitudes of the AGB stars with the shortest periods.

The positions of AGB stars, whose absolute magnitudes are confined to a range of ∼2 mag, lie in a relatively well defined band of the $(H - K_S, K_S)$ diagram whose slope results from the combined effect of extinction and distance on the apparent K_S magnitude. The fact that the scatter within this band is of the order of the scatter in the absolute magnitudes of Miras and semiregular variables suggests that the amount of reddening in the $H - K_S$ color can be used as a rough distance indicator. The intrinsic colors of Mira variables are somewhat uncertain: Glass et al. (1995) find noticeable differences in intrinsic colors when comparing Miras in the Large Magellanic Cloud, the solar neighbourhood, and the galactic bulge. They find intrinsic $H - K$ colors of bulge Miras (in the SAAO system) that range between 0.32 and 0.61, which is redder than the reddest RGB stars (Houdashelt et al. 2000) and supergiants (Ducati et al. 2001). Therefore, assuming the reddening in $H - K_S$ as a proxy for the distance, RGB and supergiants having the same position in the $K_S, H - K_S$ diagram as a given AGB star should be more distant, and therefore more luminous.

The lower edge of the *locus* of our large-amplitude variables can be approximated by the straight line $K_S = 5.87 + 2.20(H - K_S)$, which allows us to define a reference magnitude K_0 as

$$K_0 = K_S - 5.87 - 2.20(H - K_S) \quad (2)$$

whose positive or negative value indicates that the star is either below or above the lower edge of the AGB band, respectively. Although it may be tempting to directly relate K_0 to M_K, it must be noted that the straight line is just a convenient approximation to describe the *locus* of AGB stars in our sample and does not have a sound physical foundation. Indeed, it is easy to show that the assumption that K_0 is simply the absolute magnitude offset by a constant requires the distance modulus to be $DM = 12.93 + 0.42E(H - K_S)$ (where $E(H - K_S)$ is the amount of reddening, the coefficient 0.42 preceding it is derived from the Rieke & Lebofsky (1985) extinction law, and the constant after the equal sign follows from the assumption that the lower edge of the AGB band is defined by stars having $M_K = -6.4$), which does not allow for distances smaller than 3.8 kpc. Still, the use of Eq. (2) allows a split of our sample between "bright" and "faint" stars taking AGB stars as an appropriate dividing line.

The fact that the bulk of the stars in our sample falls below the $K_0 = 0$ line in Fig. 14 confirms that our sample is dominated by giants. However, there are some bright stars with different amounts of reddening occupying the AGB locus but with no or weak water absorption; note in particular the group of faint, very red stars at $(H - K_S) > 2.0$. These are some of the most promising M supergiant candidates in our sample.

The vast majority of the stars in our sample cluster along the narrow strip of the $(H - K_S)$, $(J - H)$ color−color diagram that traces the reddening vector (see Fig. 15). Some stars deviate from this strip apparently occupying the region of bluer-than-normal $(J - H)$ colors at a given $(H - K_S)$ that would indicate the existence of a near infrared excess. However, these are stars with very red colors whose faint J magnitudes are near or below the confusion limit for 2MASS in the galactic plane, for which the 2MASS J-band measurement is likely to be significantly contaminated by nearby stars. We thus consider the J magnitudes as generally unreliable for very red objects, thus precluding a discussion on the infrared excesses of different classes of objects.

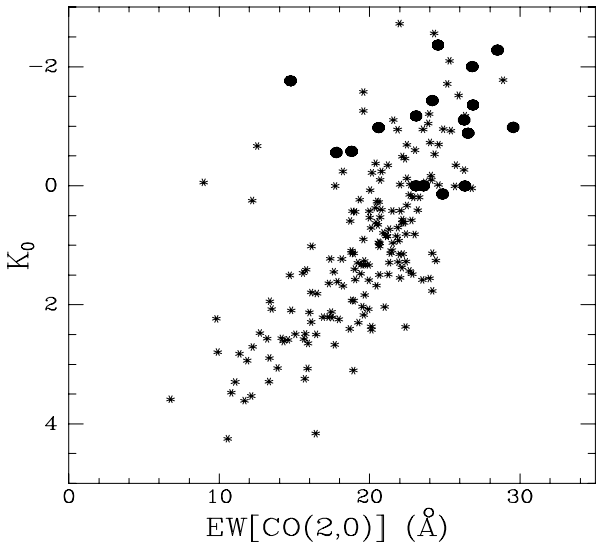

Fig. 16. EW[CO(2, 0)] vs. the K_0 quantity defined in Eq. (2) for the stars in our sample. Filled circles indicate stars with $I(H_2O) > 0$.

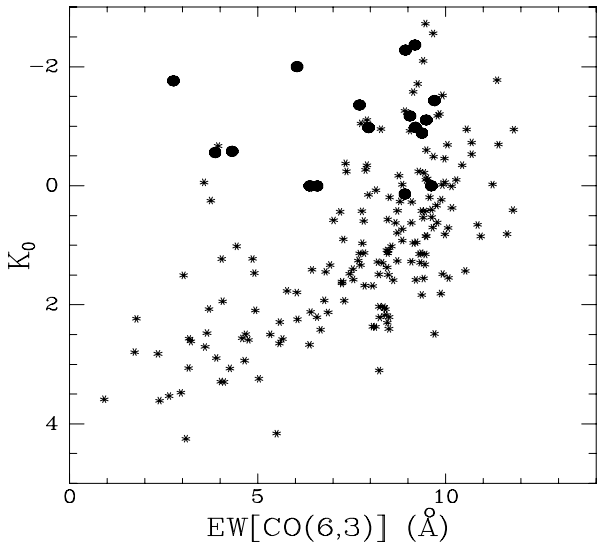

Fig. 17. Same as Fig. 6, but now with EW[CO(6, 3)] on the horizontal axis. Stars with $I(H_2O) > 0$ tend to lie to the left due to the same veiling effect on the CO(6, 3) band that causes the diagonal band in Fig. 7.

3.6. Equivalent widths and luminosities

The use of K_0 as defined in Eq. (2) allows us to study possible correlations between this quantity, purely derived from broad-band photometry, and the equivalent widths measured in the spectra. The most obvious correlations among these two quantities are shown in Figs. 16 and 17. While both figures are qualitatively similar in that they show an increase of average luminosity with increasing CO band depth, there are some interesting differences between them. The CO(2, 0) band depth vs. K_0 diagram shows an approximately constant slope, with considerable scatter, over the whole range of equivalent widths covered by our spectra. Figure 17, however, shows a break in the trend around EW[CO(6, 3)] $\simeq 7$ Å with the distribution of points flaring up to brighter values of K_0. The clear displacement of the average distribution of stars with strong water absorption towards lower EW[CO(6, 3)] is a direct consequence of the fact, mentioned earlier (see also Fig. 7) that strong water absorption is correlated with weak CO(6, 3) absorption, unlike what is observed in the case of the CO(2, 0) bandheads.

Less pronounced, but still obvious correlations with K_0 are found for the NaI and CaI bands. We have also looked for possible systematic effects of ratios of equivalent widths with K_0 that may provide spectroscopic discriminators, in particular the EW(CO(2, 0))/(EW(CaI) + EW(NaI)) ratio that Ramírez et al. (1997) proposed to discern between dwarfs and giants. The usefulness of that ratio in discriminating also between giants and supergiants is suggested by the results of Förster-Schreiber (2000), and has been investigated by Schultheis et al. (2003) for their galactic center sample. Unfortunately we can only confirm the negative results of Schultheis et al. (2003), at least at the resolution common to our spectra, in which no hint of a systematic trend with the luminosity indicator K_0 is seen.

Other absorption features appearing in our spectra such as the MgI (2.281 μm) or FeI (2.228 μm) lines may also be useful indicators of temperature, metallicity, or surface gravity. In particular we have attempted to use EW[CO(2, 0)]/EW[MgI] as a possible surface gravity indicator based on the results of Förster-Schreiber (2000), which suggest two different characteristic values of that ratio for giants and supergiants at the coolest temperatures. Again we find no systematic trend in our results, although its possible existence may be hidden due to the weakness of the MgI feature that comes close to the typical ±0.5 Å uncertainty in our equivalent width measurements, thus introducing a large random scatter in the ratios that we can determine. Similar uncertainties due to the measurement errors relative to the small equivalent widths affect measurements involving the other lines, such as FeI (2.228 μm) or SiI (1.590 μm).

LW2000 have noted that the strong CN features appearing shortwards of 1.1 μm are characteristic of the supergiants of their sample. Unfortunately that spectral region is too heavily obscured in the majority of our sources, thus preventing measurement of the strongest CN bands. However, there are multiple CN features appearing on the bluer side of the K band that may provide a useful alternative in heavily reddened objects. We find hints of a surface gravity dependence in the blend of CN lines near 2.134 μm, as shown in Fig. 18. Again, the weakness of the feature prevents its accurate measurement in many of our spectra, but higher resolution and S/N spectra might prove this to be an efficient way of producing clean samples of giants or supergiants. We note that the comparison of CN and CO absorption bands provides measurements of surface abundances of CNO-processed elements; this has important implications for the internal structure and dredge-up history of the objects under study (Carr et al. 2000; see also Sect. 4).

3.7. Defining a sample of candidate supergiants

As discussed in the previous sections, we have failed to find in our spectra a discontinuity between the properties of giants and supergiants that would have allowed a clear

discrimination between the two groups. Moreover, very few objects in our sample display simultaneously weak or absent H_2O absorption wings and very strong CO(2, 0) absorption in the range covered by the supergiants of LW2000, thus suggesting that supergiants with spectroscopic characteristics closely matching those of the local sample are not present in large numbers among the stars that we observed. Nevertheless, we do find many stars with NaI absorption similar or greater than those of local supergiants, no signs of H_2O absorption wings, moderate but not extreme CO(6, 3) and CO(2, 0) absorption, and photometric characteristics that suggest an intrinsic luminosity exceeding that of the brightest giants. These properties lead us to suspect that our sample does contain a number of cool supergiants in the inner Galaxy whose spectroscopic characteristics present systematic differences with respect to local supergiants, being in fact closer to those of the galactic center supergiants, as noted in Sect. 3.5; see also Sect. 4.1. Taking together the indicators referred to above, we have produced a list of candidate supergiants in the inner Galaxy composed by the stars in our sample that fulfill the following criteria:

- $I(H_2O) < -0.1$, denoting the absence of significant H_2O absorption wings. The negative threshold is quite restrictive, as weak water absorption is common among the coolest supergiants (Lançon & Rocca-Volmerange 1992) and the $I(H_2O)$ values of the typical Mira-like spectra in our sample reach several tenths above zero. As a matter of fact, as many as seven of the LW2000 supergiant spectra would *not* be considered as supergiant candidates on the grounds of this criterion (see Fig. 6).
- EW[NaI] > 4 Å, thus selecting as supergiant candidates objects with an NaI feature stronger than that of the coolest giants in metal-rich globular clusters and in the solar neighbourhood.
- EW[CO(2, 0)] > 19 Å and EW[CO(6, 3)] > 7 Å. We have already pointed out that these thresholds are well below the typical strengths of the CO features in the local supergiants, but they correspond to the values for which stars with $K_0 < 0$ appear in Figs. 16 and 17. As we will discuss in Sect. 4, the possibility that the CO features are systematically weaker among bright cool stars in the inner Galaxy makes it advisable to use not-too-restrictive criteria on the CO features.
- $K_0 < -0.1$, to select stars whose broad-band photometry suggests high luminosity. The usefulness and limitations of K_0 as a luminosity indicator have been discussed in Sect. 3.5, and we stress again that K_0 is expected to be only loosely correlated with the absolute magnitude. We consider it however as a useful additional indicator of the possible supergiant nature of our candidates when used in combination with the other criteria described in this section. The threshold chosen is intended to exclude stars that may have been placed above the $K_0 = 0$ line by inaccuracies in the photometry.

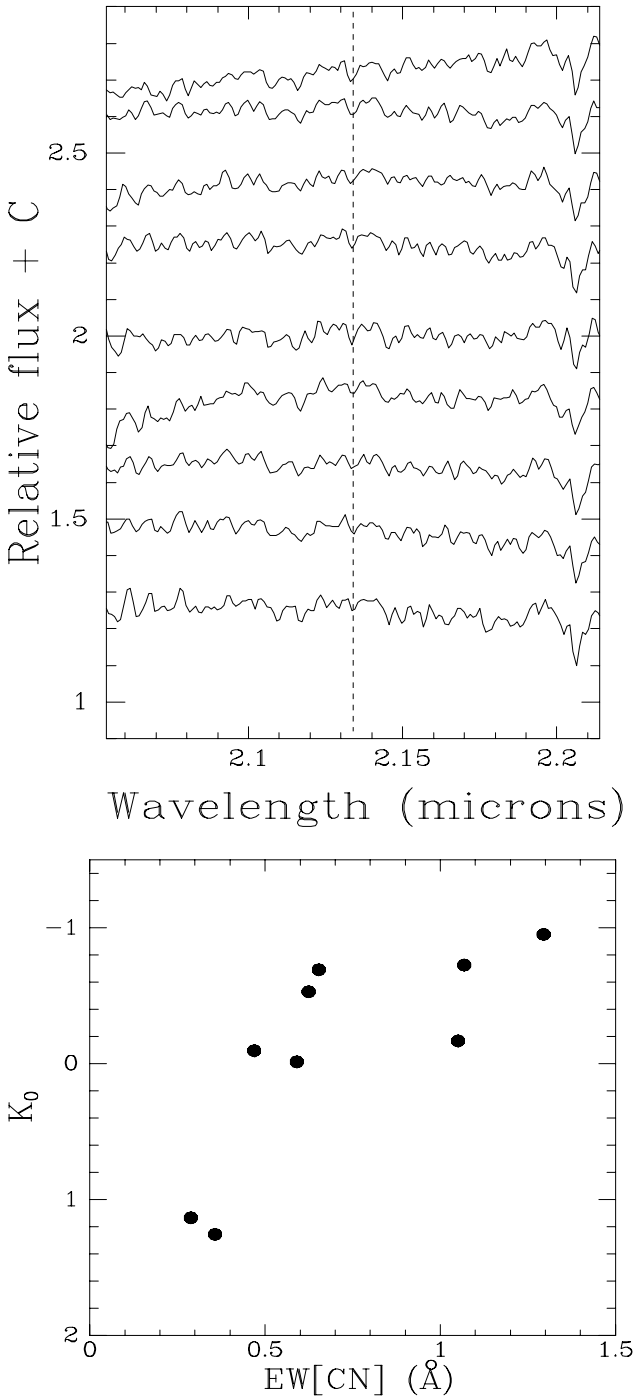

Fig. 18. A possible luminosity effect in the CN bands? In the top panel, spectra are sorted by the value of K_0 (Eq. (2)), with the most negative values (implying on the average more luminous stars) at the top. The CN feature, marked by the dashed line, has a trend to be stronger in the most luminous stars. The stars plotted here are the ones in our sample for which we measure $24 < EW$[CO(2, 0)] < 25, to remove possible temperature effects on the CN bands. However, such a trend is not confirmed for the general sample. The bottom panel shows the equivalent width vs. K_0, quantifying the effect hinted at by the top panel.

The selection of the best cool supergiant candidates obtained through the application of these criteria thus contains 18 objects, listed in Table 3. We have excluded one object, Star 191, due to its relatively blue $(H - K_S) = 0.40$; as indicated in Sect. 14 the rough correlation between broad-band colors and luminosity given by Eq. (2) must break down for blue colors

indicative of low extinction, and the characteristics of Star 191 are well compatible with those of a lightly reddened, nearby RGB star. It is interesting to note as a validation of these criteria that 7 out of the 8 reddest stars in our sample, which are heavily obscured but still bright enough to be in our sample and are thus good supergiant candidates based on their photometric properties alone, do fulfill all the spectroscopic criteria as well. Likewise, Star 011, which is the one that best matches the spectral characteristics of the LW2000 sample of M supergiants, is also included in our selection as a moderately reddened star and thus probably not very distant, as may be expected from an object whose properties are similar to those of the local sample.

As noted above, the criterion based on the almost complete absence of H_2O absorption wings is deliberately conservative, as the coolest local supergiants do show moderate absorption. We thus provide in Table 4 an additional list of M supergiant candidates, with a lower level of confidence than those provided in Table 3, with weak H_2O absorption. Such a table would contain most LW2000 local supergiants as well, although their EW[CO(2, 0)] would be greater on average.

The K_S magnitudes of most objects in Tables 3 and 4 and the reddenings implied by their $H - K_S$ are consistent with distances to the Sun placing them well within the solar circle, given the expected absolute K magnitudes of cool supergiants. However, this may not be true for the faintest, most reddened sources in those tables. For instance, assuming $M_K = -11$ (which is very bright, although not unrealistic for a M supergiant; Elias et al. 1985) and $(H-K_S)_0 = 0.3$ for Star 072 would place it at 17.1 kpc from the galactic center on the opposite side of the solar circle, assuming a galactocentric distance of the Sun of 8 kpc, and obscured by $A_V \simeq 35$ mag. Nevertheless, most of the other candidate supergiants are both brighter in the K band and less reddened, and the assumption that they are indeed located in the inner galactic disk can be expected to be generally valid. This is even more so for the RGB stars of our sample, whose absolute magnitudes are fainter.

4. Discussion

4.1. Cool giants and supergiants in the galactic center

Differences similar to those that we have discussed in the previous sections between our sample of cool luminous stars and local samples have already been noted in previous studies of the galactic bulge, as already discussed in Sect. 3.4, as well as of the galactic center. The latter are of particular interest, since they include supergiants in addition to RGB stars. Early infrared investigations of the stellar population at the galactic center revealed a high density of cool, luminous stars including supergiants and giants (Lebofsky et al. 1982; Sellgren et al. 1987). Similar to their hotter counterparts, the comparison of properties of cool massive stars in the galactic center with similar stars in the solar neighbourhood has been the subject of intense study to investigate how the widely different environment influences their formation and evolution.

Sellgren et al. (1987; see also Blum et al. 1996) already noted that a number of galactic center giants and supergiants display unusually strong CaI and NaI features when observed at low spectral resolution. Although differences between galactic center and solar neighbourhood luminous stars have often been interpreted as due to the effects of metallicity on stellar evolution, detailed abundance analyses have recently called this into question by showing that galactic center stars have metallicities very close to solar values (Carr et al. 2000 and references therein; Ramírez et al. 2000a; Blum et al. 2003).

Most interesting in the context of our results is the detailed abundance analysis performed by Carr et al. (2000) on IRS 7, the brightest M supergiant in the galactic center. While spectroscopy at a resolution similar to ours also shows strong CaI, NaI features for this star, its CO band at 2.293 μm is found to be significantly weaker than those of the local M supergiants α Ori and VV Cep, whose temperatures are very similar to that of IRS 7 as shown by model atmosphere fits. The study of Carr et al. (2000) reveals a strong surface depletion of C and O and a corresponding enhancement of N with respect to local supergiants, while the combined abundance of C, N, and O adds to a value close to solar. Such altered abundances not only explain the weaker CO features (whose strength is essentially determined by the C abundance in O-rich atmospheres), but also the unusual strength of the NaI and CaI features in low resolution ($R \simeq 1000$) spectra. Indeed, high resolution spectroscopy reveals that these atomic features are strongly contaminated by a large number of CN bands, which can even dominate the contribution to the feature in the coolest stars (Ramírez et al. 1997). The enhancement in the surface abundances of CNO-processed elements has the net effect of increasing the contribution of CN to the observed NaI and CaI features.

The interpretation given by Carr et al. (2000) invokes deep mixing enhanced by fast stellar rotation as the explanation for the difference between galactic center and local supergiants. They also suggest that higher rotation velocities on the average, caused by the extreme prevailing conditions for star formation, could also explain the differences observed in other classes of high mass stars at the galactic center without requiring metallicities higher than solar. A similar explanation may also apply to the galactic center giants whose low-resolution spectral properties are also comparable.

As noted in Sect. 3.5, four more *bona fide* supergiant candidates have recently been identified among ISOGAL sources near the galactic center by Schultheis et al. (2003). Their classification as supergiants is based on the estimated absolute magnitude and the absence of water absorption. Three of these stars have EW[CO(2, 0)] in the 20−24 Å interval, well within the range covered by the supergiant candidates in our sample and also by local RGB stars. The fourth has EW[CO(2, 0)] < 28 Å, which is also well below those of most local supergiants in LW2000 sample. These results thus support the trend of galactic center supergiants to have CO bands weaker than those of local supergiants.

4.2. Metallicity and systematic differences in feature strengths

It is extremely unlikely that an explanation based on rotation such as the one proposed by Carr et al. (2000) can also account

for the properties of our inner Galaxy sample, since the formation conditions at distances of a few kiloparsecs from the galactic center should be much closer to those in the solar neighbourhood and no reason why our stars should be faster rotators is apparent. However, we note that the constraint of explaining the peculiar features of galactic center stars while not invoking supersolar metallicity most probably does not apply to our sample, which populates a region of the galactic disk where the existence of a higher average metallicity is well established by a wide variety of tracers; see Chiappini et al. (2001) for an exhaustive summary of galactic abundance gradient determinations for different elements. It is in fact very difficult to disentangle the effects of high metallicity from those of fast rotation on stellar evolution, and in particular on mixing in the interior of the star, as has been discussed by Schaerer (2000).

The resemblance between the distinctive properties of galactic center stars and those of our sample (greater strength of the CaI and NaI features, comparative weakness of the K-band CO absorption relative to similar stars in the solar neighbourhood) leads us to consider it very plausible that the spectroscopic features of many of our stars can also be explained by the enhanced abundance of CNO-processed material in the stellar surface resulting from deep mixing, as suggested by Carr et al. (2000) for IRS 7 and possibly other galactic center objects. However, the fact that our stars most likely have a higher average metallicity than those of the solar neighbourhood and also those of the galactic center leads us to consider metallicity, rather than rotation, as the reason for the enhanced surface CNO element abundance. Higher metallicity implies higher opacity in the interior of the star, leading to a deeper penetration of the outer convective zone during the first dredge-up (Vandenberg & Smith 1988; Gratton et al. 2000). In turn higher mass loss rates, enhanced by the higher metallicity, may also play a role by efficiently removing the outer envelope and rapidly make visible at the surface deep layers whose composition has been altered by CNO reactions (G. Meynet, priv. comm.)

In view of our results and the above discussion, we refrain from deriving quantitative properties of our stars from the available spectroscopic material using extrapolations of relationships calibrated for populations considerably different from ours, such as the metallicity calibration of Frogel et al. (2001) or the EW[CO(2, 0)]-based temperature scale proposed by Ramírez et al. (1997). We find it necessary to defer a tentative determination of the intrinsic properties of our sample (temperatures, metallicities, surface gravities, absolute luminosities...) to future work based on high resolution spectroscopy, which should allow quantitative analyses based on detailed atmosphere and stellar evolution models.

5. Summary and conclusions

In this paper we have presented the results of a search for cool, luminous stars in the inner region of the Milky Way ($6^\circ < l < 21^\circ$), selected by the signature of their strong CO bandheads longward of $\lambda = 2.293$ μm in narrow-band imaging. Low resolution spectroscopy has been presented for 191 stars confirmed to have moderate or strong CO bands and other signatures of cool spectra. Some of these stars are readily classified as large-amplitude variable candidates from the appearance of broad H_2O absorption wings. Our spectra also allow the measurement of a number of atomic and molecular features in the H and K bands. The addition of near-infrared photometry from 2MASS, which is available for all the stars in our sample, allows us to estimate rough luminosities. We find that our sample is dominated by red giant branch stars, but the photometric characteristics of some stars suggests luminosities in the range covered by the intrinsically more luminous large-amplitude variables, suggesting that they are red supergiants. The spectroscopic characteristics are consistent with such classification.

We have compared the spectroscopic results obtained for our sample with those derived from the atlas of near-infrared spectra of cool luminous stars of Lançon & Wood (2000), which is mostly composed of stars in the solar neighbourhood and bulge red giants, as well as with the samples of nearby red giants of Ramírez et al. (1997) and bulge giants of Ramírez et al. (2000b). We have also made a comparison with a sample of red giants in globular clusters with metallicities in the $-0.37 <$ [Fe/H] < -0.17 from Frogel et al. (2001). The results of these comparisons may be summarized as follows:

- The local sample of red supergiants displays spectra with CO bands significantly stronger than those of the stars in the inner Galaxy sample, especially the CO(2, 0) band. The difference is less pronounced for the CO(6, 3) band, where there is significant overlap between our sample and the local one. We find only one star in our sample whose EW[CO(2, 0)] is well within the range of those of local supergiants.
- The CaI and NaI features in the K band are on the average as strong as, or even stronger than, those of local supergiants. As compared to local and globular cluster RGB stars, most stars in our sample have EW[CaI] and, especially, EW[NaI] well exceeding those of the coolest stars in those samples. However, similarly strong CaI and NaI features are observed among bulge giants. The net result of this effect and the one described in the previous item is a well defined shift of the band defined by our sample in the EW[CaI] vs. EW[CO(2, 0)] or the EW[NaI] vs. EW[CO(2, 0)] with respect to the average *loci* of the reference samples of the solar neighbourhood.
- An application of combined photometric and spectroscopic criteria allows us to define a sample of 18 good M supergiant candidates having no noticeable H_2O absorption, strong CO absorption both in the H and K bands, and H, K_S photometry similar to that of large amplitude variables, suggesting that they are also intrinsically very luminous. Most of them are considerably reddened by extinction reaching up $A_V \simeq 40$ mag. Nine additional candidates with weak H_2O absorption wings are also identified.
- A comparison between the spectroscopic characteristics at low resolution of our best supergiant candidates and of the rest of stars in our sample confirms results of other authors about the unsuitability of spectra at $R \simeq 1000$ or lower to clearly discern between red giants and supergiants,

complicated with the interpretation of the measurements of the CO and atomic features, and in particular the actual species that contribute to the latter.

The discussion of our results (Sect. 4) is centered on the fact that the low-resolution characteristics noted in our sample and summarized above (strong NaI and CaI features, probably due to their contamination by CN lines, and comparatively weak CO absorption) are shared by giants and supergiants in the vicinity of the galactic center. We have referred to detailed abundance analyses by other authors of the galactic center stars, which indicate solar metallicities but altered surface abundances of CNO-processed elements with respect to local supergiants, resulting in depleted C and O and enhanced N. Systematic differences in rotational velocities, implying deeper mixing in galactic center stars, are invoked to account for the different surface abundances while keeping a solar metallicity. While we find that systematically different rotation velocities are extremely unlikely to account for the observed differences, we still consider that deeper mixing and the resulting patterns in surface abundances are an attractive explanation of the characteristics of our sample. We propose that higher metallicities in the inner regions of the Galaxy are responsible for the deep mixing, probably as a consequence of the increased interior opacity.

Higher resolution spectroscopy in the infrared (the only spectral region accessible for the study of the photospheres of such heavily reddened objects) will be needed to perform detailed abundance analyses as well as to separate giants and supergiants in a more reliable way than was possible with the material currently available. Nevertheless, interesting conclusions may already be drawn from our work. On the one hand, we confirm the feature, already suspected from studies of galactic center stars, that very strong CO absorption longwards of 2.293 μm is a distinctive property of local supergiants but may not apply to supergiants in other environments. On the other hand, the usefulness of local giants and supergiants as templates for population synthesis studies must be regarded with some caution taking into account our results and the ones referred to on the galactic center. Indeed, common domains of application of population synthesis are central starbursts and the stellar environments of AGNs, where the conditions for star formation and evolution may be better represented by those in the inner regions or the center of the Milky Way. The identification of a large sample of cool, luminous field stars such as the one presented in this paper is a necessary first step towards the understanding of their physical and chemical properties that may emerge from the combination of future high resolution observations and detailed modelling. Such work will provide a useful database for improving our knowledge of the star forming history and chemical evolution of the inner galactic disk in the proximity of the galactic plane, or of a variety of extragalactic environments where large scale massive star formation is taking place.

Acknowledgements. We are pleased to acknowledge the Calar Alto time allocation committee for the generous amount of time assigned to this project. Our special thanks to the Calar Alto staff for their excellent support during the observations. We are also pleased to acknowledge the support received at the La Silla observatory during our SOFI run, especially from Ms. Karla Aubel and Dr. Olivier Hainaut, and the warm hospitality of the ESO Guesthouse in Santiago where much of the spectroscopic data reduction was carried out. We are thankful to Dr. Ana E. Gómez for her participation in one on the Calar Alto observing runs and for her comments on early drafts of this paper. The insightful comments of Dr. G. Meynet on the role of the metallicity in producing the spectral differences discussed here are greatly appreciated. We also thank the referee, Dr. John Carr, for his constructive report that greatly helped us to improve the contents of this paper in many places. CC acknowledges the support of the Visiting Scientists Program at ESO for making possible her stay in Garching, during which part of this work was done, and financial support from MIUR/COFIN 2003028039. J.T., F.F., and S.R. acknowledge support from the MCYT under contract AYA2003-007736. This publication makes use of data products from the Two Micron All Sky Survey, which is a joint project of the University of Massachusetts and the Infrared Processing and Analysis Center/California Institute of Technology, funded by the National Aeronautics and Space Administration and the National Science Foundation.

References

Alard, C. 2001, A&A, 379, L44
Alonso-Herrero, A., Engelbracht, C. W., Rieke, M. J., Rieke, G. H., & Quillen, A. C. 2001, ApJ, 546, 952
Becker, R. H., White, R. L., Helfand, D., & Zoonematkermani, S. 1994, ApJS, 91, 347
Bessell, M. S., Brett, J. M., Wood, P. R., & Scholz, M. 1989, A&A, 213, 209
Blum, R. D., Sellgren, K., & DePoy, D. L. 1996, AJ, 112, 1988
Blum, R. D., Ramírez, S. V., Sellgren, K., & Olsen, K. 2003, ApJ, 597, 323
Bronfman, L., Nyman, L.-Å., & May, J. 1996, A&AS, 115, 81
Bronfman, L., Casassus, S., May, J., & Nyman, L.-Å. 2000, A&A, 358, 521
Bruzual, G., & Charlot, S. 2003, MNRAS, 344, 1000
Carr, J. S., Sellgren, K., & Balachandran, S. C. 2000, ApJ, 530, 307
Chiappini, C., Mateucci, F., & Romano, D. 2001, ApJ, 554, 1044
Chiar, J. E., Kutner, M. L., Verter, F., & Leous, J. 1994, ApJ, 431, 658
Codella, C., Palumbo, G. G. C., Pareschi, G., et al. 1995, MNRAS, 276, 57
Comerón, F., & Torra, J. 1996, A&A, 314, 776
Dallier, R., Boisson, C., & Joly, M. 1996, A&AS, 116, 239
Dame, T. M., Ungerechts, H., Cohen, R. S., et al. 1987, ApJ, 322, 706
Dame, T. M., Hartmann, D., & Thaddeus, P. 2001, ApJ, 547, 792
Ducati, J. R., Bevilacqua, C. M., Rembold, S. B., & Ribeiro, D. 2001, ApJ, 558, 309
Egan, M. P., Shipman, R. F., Price, S. D., et al. 1998, ApJ, 494, L199
Elias, J. H., Frogel, J. A., & Humphreys, R. M. 1985, ApJS, 57, 91
Ferraro, F. R., Montegriffo, P., Origlia, L., & Fusi Pecci, F. 2000, AJ, 119, 1282
Fioc, M., & Rocca-Volmerange, B. 1997, A&A, 326, 950
Förster-Schreiber, N. M. 2000, AJ, 120, 2089
Förster-Schreiber, N. M., Genzel, R., Lutz, D., Kunze, D., & Sternberg, A. 2001, ApJ, 552, 544
Frogel, J. A., Stephens, A., Ramírez, S., & DePoy, D. L. 2001, AJ, 122, 1896
Green, D. A. 1991, PASP, 103, 209
Green, D. A. 2001, A catalogue of galactic supernova remnants, Mullard Radio Astronomy Observatory, Cambridge

Glass, I. S., Whitelock, P. A., Catchpole, R. M., & Feast, M. W. 1995, MNRAS, 273, 383
Gratton, R. G., Sneden, C., Carretta, E., & Bragaglia, A. 2000, A&A, 354, 169
Helfand, D. J., Zoonematkermani, S., Becker, R. H., & White, R. L. 1992, ApJS, 80, 211
Hinkle, K., Wallace, L., & Livingston, W. 1995, PASP, 107, 1042
Houdashelt, M. L., Bell, R. A., & Sweigart, A. V. 2000, AJ, 119, 1448
Hughes, V. A., & MacLeod, G. C. 1994, ApJ, 427, 857
Ivanov, V. D., Rieke, M. J., Engelbracht, C. W., et al. 2004, ApJS, 151, 387
Kleinmann, S. G., & Hall, D. N. B. 1986, ApJS, 62, 501
Knapp, G. R., Pourbaix, D., Platais, I., & Jorissen, A. 2003, A&A, 403, 993
Kolpak, M. A., Jackson, J. M., Bania, T. M., Clemens, D. P., & Dickey, J. M. 2003, ApJ, 582, 756
Kotilainen, J. K., Forbes, D. A., Moorwood, A. F. M., van der Werf, P. P., & Ward, M. J. 1996, A&A, 313, 771
Kuchar, T. A., & Bania, T. M. 1994, ApJ, 436, 117
Lançon, A., & Rocca-Volmerange, B. 1992, A&AS, 217, 271
Lançon, A., & Wood, P. R. 2000, A&AS, 146, 217
Leahy, D. A., & Wu, X. 1989, PASP, 101, 607
Lebofsky, M. J., Rieke, G. H., & Tokunaga, A. T. 1982, ApJ, 263, 736
Livingston, W., & Wallace, L. 1991, An atlas of the solar spectrum in the infrared from 1850 to 9000 cm^{-1} (1.1 to 5.4 μm), NSO Technical Report, NOAO
Lockman, F. J. 1989, ApJS, 71, 469
López-Corredoira, M., Garzón, F., Beckman, J. E., et al. 1999, AJ, 118, 381
López-Corredoira, M., Hammersley, P. L., Garzón, F., et al. 2001, A&A, 373, 139
López-Corredoira, M., Cabrera-Lavers, A., Garzón, F., & Hammersley, P. L. 2002, A&A, 394, 883
Maiolino, R., Rieke, G. H., & Rieke, M. J. 1996, AJ, 111, 537
Mathis, J. S. 1990, ARA&A, 28, 37
McClure-Griffiths, N. M., Green, A. J., Dickey, J. M., et al. 2001, ApJ, 551, 394
McQuinn, K. B. W., Simon, R., Law, C. J., et al. 2002, ApJ, 576, 274
Meyer, M. R., Edwards, S., Hinkle, K. H., & Strom, S. E. 1998, 508, 397
Ojha, D. K. 2001, MNRAS, 322, 426
Omont, A. 1996, ASP Conf. Ser., 102, 305
Origlia, L., Moorwood, A. F. M., & Oliva, E. 1993, A&A, 280, 536
Origlia, L., & Oliva, E. 2000, A&A, 357, 61
Picaud, S., Cabrera-Lavers, A., & Garzón, F. 2003, A&A, 408, 141
Ramírez, S. V., DePoy, D. L., Frogel, J. A., Sellgren, K., & Blum, R. D. 1997, AJ, 113, 1411
Ramírez, S. V., Sellgren, K., Carr, J. S., et al. 2000a, ApJ, 537, 205
Ramírez, S. V., Stephens, A. W., Frogel, J. A., & DePoy, D. L. 2000b, AJ, 120, 833
Rieke, G. H., & Lebofsky, M. J. 1985, ApJ, 288, 618
Ruphy, S., Epchtein, N., Cohen, M., et al. 1997, A&A, 326, 597
Schaerer, D. 2000, in Stars, Gas and Dust in Galaxies: Exploring the Links, ASP Conf. Ser., 221, 99
Schultheis, M., Lançon, A., Omont, A., Schuller, F., & Ojha, D. K. 2003, A&A, 405, 531
Sellgren, K., Hall, D. N. B., Kleinmann, S. G., & Scoville, N. Z. 1987, ApJ, 317, 881
Stetson, P. B. 1987, PASP, 99, 191
Sweigart, A. V., Greggio, L., & Renzini, A. 1990, ApJ, 364, 527
Unavane, M., & Gilmore, G. 1998, MNRAS, 395, 145
van Loon, J. Th., Gilmore, G. F., Omont, A., et al. 2003, MNRAS, 338, 857
Vandenberg, D. A., & Smith, G. H. 1988, PASP, 100, 314
Wallace, L., & Hinkle, K. 1996, ApJS, 107, 312
Wallace, L., & Hinkle, K. 1997, ApJS, 111, 445
Whiteoak, J. B. Z. 1992, A&A, 262, 251
Wood, D. O. S., & Churchwell, E. 1989, ApJ, 340, 265